Sensory experience controls dendritic structure and behavior by distinct pathways involving degenerins

Sharon Inberg[1], Yael Iosilevskii[1], Alba Calatayud-Sanchez[2], Hagar Setty[3,4], Meital Oren-Suissa[3,4], Michael Krieg[2], and Benjamin Podbilewicz[1,*]

[1]Department of Biology, Technion-Israel Institute of Technology, 3200003 Haifa, Israel

[2]ICFO - Institut de Ciencies Fotoniques, The Barcelona Institute of Science and Technology, Castelldefels (Barcelona) 08860, Spain

[3]Department of Brain Sciences, Weizmann Institute of Science, Rehovot 7610001, Israel

[4]Department of Molecular Neuroscience, Weizmann Institute of Science, Rehovot 7610001, Israel

* Corresponding author
Department of Biology,
Technion-Israel Institute of Technology, 3200003 Haifa, Israel
Tel +972 4 8293454
Email: podbilew@technion.ac.il

Competing Interest Statement: None

Classification: Biological Sciences. Neuroscience

Keywords: Dendritic plasticity, *Caenorhabditis elegans,* Epithelial sodium channels (degenerins)

This file includes:

- Main Text
- Figure Legends
- Supplementary Figure Legends
- Video Legends
- Supplementary File Legend
- Titles for the Source Data

Abstract

Dendrites are crucial for receiving information into neurons. Sensory experience affects the structure of these tree-like neurites, which, it is assumed, modifies neuronal function, yet the evidence is scarce, and the mechanisms are unknown. To study whether sensory experience affects dendritic morphology, we use the *Caenorhabditis elegans'* arborized nociceptor PVD neurons, under natural mechanical stimulation induced by physical contacts between individuals. We found that mechanosensory signals induced by conspecifics and by glass beads affect the dendritic structure of the PVD. Moreover, developmentally isolated animals show a decrease in their ability to respond to harsh touch. The structural and behavioral plasticity following sensory deprivation are functionally independent of each other and are mediated by an array of evolutionarily conserved mechanosensory amiloride-sensitive epithelial sodium channels (degenerins). Calcium imaging of the PVD neurons in a micromechanical device revealed that controlled mechanical stimulation of the body wall produces similar calcium dynamics in both isolated and crowded animals. Our genetic results, supported by optogenetic, behavioral, and pharmacological evidence, suggest an activity-dependent homeostatic mechanism for dendritic structural plasticity, that in parallel controls escape response to noxious mechanosensory stimuli.

Significance Statement

Little is known about how neuronal activity and sensory experience influence the structure and function of dendritic trees. Furthermore, how dendritic structures affect neuronal functions remains to a large extent a mystery despite their fundamental functions in neuronal sensory and synaptic activities in health and diseases. Here we show that complex dendritic trees of the nociceptive and proprioceptive PVD neuron in *C. elegans* display a dynamic nature where they undergo pronounced dendritic modifications during adulthood. These modifications are determined by the received sensory signals generated by conspecific worms on the plate or by inert glass beads. We revealed functions for degenerins/Epithelial sodium channels in this phenomenon, using genetic and optogenetic approaches. We found that the degenerin MEC-10 acts cell autonomously to translate environmental mechanical signals into structural and functional modifications in the PVD.

Main Text

Introduction

The general structure of the nervous system has been known for over a century. Groundbreaking studies on synaptic plasticity and its underlying mechanisms have shown that before birth and in adult animals, neuronal activity is needed for synaptic remodeling (Fox and Wong, 2005, Goodman and Shatz, 1993, Katz and Shatz, 1996, Wiesner et al., 2020, Zuo et al., 2005). In contrast, the molecular mechanisms responsible for structural remodeling of dendritic trees, as a result of different sensory inputs (experience), especially during adulthood, are less understood (Kolb and Whishaw, 1998, Tavosanis, 2012, Wong and Ghosh, 2002).

Mechanistic understanding of experience-dependent structural plasticity is primarily focused on activity sensation by calcium channels and N-methyl-D-aspartate (NMDA) receptors. These are known to induce downstream signaling cascades affecting, among others, the Rho family of small GTPases, calcium metabolism and microtubule stability (Ghiretti et al., 2014, Sin et al., 2002, Vaillant et al., 2002, Zhou et al., 2006). Several neurological conditions including autism, Down syndrome, fragile X syndrome, and schizophrenia are characterized by abnormal dendritic spine structures (Hu et al., 2020, Huebschman et al., 2020, Jan and Jan, 2010, Tendilla-Beltran et al., 2019). Uncovering the molecular basis of dendritic tree instability during development and adulthood, may shed light on neurological disease mechanisms and elucidate their behavioral phenotypes.

The dendrite morphology of the *Caenorhabditis elegans'* PVD bilateral neurons is composed of repetitive, stereotypical and spatially organized structural units that resemble candelabra (Figure 1A), making it a useful platform to study dendritic morphogenesis in hermaphrodites and males (Oren-Suissa et al., 2010; Iosilevskii and Podbilewicz, 2024; for a review see (Heiman and Bülow, 2024)). While some of the genetically-programmed molecular mechanisms responsible for the morphogenesis and regeneration of PVD's dendritic trees are known (Dong et al., 2013, Dong et al., 2015, Inberg et al., 2019, Kravtsov et al., 2017, Oren-Suissa et al., 2017, Oren-Suissa et al., 2010, Salzberg et al., 2013, Salzberg et al., 2014, Smith et al., 2010; Heiman and Bülow, 2024), the influence of nurture (e.g. sensory experience) on its structure and function remain unexplored. The PVD mediates several sensory modalities (reviewed in (Goodman and Sengupta, 2019)), notably response to harsh mechanical stimuli (nociception) (Chatzigeorgiou et al., 2010), response to low temperatures (Chatzigeorgiou et al., 2010) and proprioception (Albeg et al., 2011, Tao et al., 2019, reviewed in Krieg, et. al., 2022). While the PVD response to low temperatures is mediated by transient receptor potential (TRP) channels (Chatzigeorgiou et al., 2010), nociception and proprioception are mediated by Degenerins/Epithelial sodium (Na^+) Channels (DEG/ENaCs) expressed in the PVD (Chatzigeorgiou et al., 2010, Husson et

al., 2012), which form homo- and hetero-trimers and are involved in force sensing. In mammals, some DEG/ENaCs such as ASIC1a participate in synaptic plasticity and cognitive functions such as learning and memory (Baldin et al., 2020, Bianchi and Driscoll, 2002, Chen et al., 2015, Gillespie, 2001, Gobetto et al., 2021, Hill and Ben-Shahar, 2018, Mango and Nistico, 2020, Welsh et al., 2002). As sensory and social isolation affect the behavior and fitness of diverse animals (Bailey and Moore, 2018, Kuhlman et al., 2014, Wilbrecht et al., 2010, Yu and Zuo, 2011), including primates (Harlow et al., 1965), studying adult nematode somatosensory neurons can reveal possibly-conserved mechanisms of dendritic plasticity, which are induced by sensory stimuli.

In gentle touch circuits, which are distinct from nociception (Chalfie and Sulston, 1981, Li et al., 2011, Oren-Suissa et al., 2010), Rose and colleagues (Rose et al., 2005) found that deprivation of mechanosensory stimulation generated by colliding conspecifics in the growing plate, resulted in modified glutamatergic signaling and reduced response to tap stimulation. Here, we adapted this mechanosensory stimulation paradigm (Rose et al., 2005), where the crowded worms are thought to represent the natural 'default' enriched mechanosensory state, to look into nociceptive circuits and identify the mechanism that couples mechanosensory experience to structural and functional dendritic plasticity (Inberg and Podbilewicz, 2018). We focused on how mechanosensory experience, perceived through DEG/ENaCs, affects structural plasticity of the PVD dendritic trees in adult *C. elegans*, and whether this entails behavioral consequences. We find that mechanosensory experience not only alters the PVD's dendritic structure in the adult, but also affects associated behavioral outputs. However, and in contrast to the prevalent hypothesis, these structural and behavioral properties are not correlated.

Results

Sensory isolation induces behavioral plasticity

Rose and colleagues (Rose et al., 2005) have shown that isolation of wildtype (WT) *C. elegans* causes a decreased response to gentle touch circuits when comparing to worms raised in a crowded setting. We utilized a similar paradigm to study nociception, a behavior associated with PVD neuron activation (Oren-Suissa et al., 2010, Way and Chalfie, 1988), using a behavioral assay that registers escape following prodding with a platinum wire (harsh touch assay; Figure 1A) (Chalfie and Sulston, 1981, Li et al., 2011, Oren-Suissa et al., 2010). To study whether mechanosensory deprivation affects the nociceptive functions of the PVD, we isolated embryos into single plates where they grew 72 h to adulthood and compared their behavioral response to harsh touch against same-aged adults that were grown on crowded plates (Figure 1B). We found that ~40% of isolated WT animals responded to harsh touch, compared with ~80% of animals grown in crowded plates (Figure 1C). To test whether gentle touch neurons are involved

in this behavioral difference, we studied *mec-4(e1611)* mutants, in which gentle touch neurons are degenerated (Caneo et al., 2019, Driscoll and Chalfie, 1991, Hedgecock et al., 1983, Li et al., 2011, Suzuki et al., 2003), and obtained similar results (Figure 1C). Given that *mec-4(e1611)* exhibits the same experience-dependent behavioral plasticity as WT, we conclude that this phenomenon is independent from the *mec-4* gentle-touch neurons. As a negative control, we used *mec-3(e1338)* mutants, that are harsh-touch-insensitive (Way and Chalfie, 1988) and found no responses for both groups (Figure 1C). Thus, isolation reduces the response to noxious stimuli, in a process that is independent of gentle touch circuits.

To determine whether the effect of isolation on nociception is related to the mechanosensory deficit itself (absence of channel gating to detect collisions (Shi et al., 2016; Chatzigeorgiou et al., 2010)), in contrast to chemosensory stimuli, we used the *mec-4* strain to compare responses of isolated worms to responses of isolated worms grown in the presence of glass beads (resembling a method used by (Sawin et al., 2000)). Worms grown in isolation with beads had a similar response compared to animals grown in crowded plates (Figure 1–figure supplement 1A). While the beads are sufficient to increase isolated animals' responses, they do not fully recapitulate the crowded state (Figure 1–figure supplement 1A). To study whether the effect was chemosensory-mediated, we tested plates pre-stimulated with pheromones as well as *osm-6* mutants (defective in olfactory sensory cilia (Collet et al., 1998)). We found that isolation induced a reduction in the response to harsh touch, regardless of plate 'odor' (Figure 1D) or chemosensory function (Figure 1–figure supplement 1B). We note that the chemosensory defective *osm-6* mutants also have a defective ciliated mechanosensory PDE neuron (Collet et al., 1998) (which also mediates posterior harsh touch responses (Li et al., 2011)). These results suggest that adult worms display a behavioral plasticity in PVD-related harsh touch circuits, which is dependent on mechanosensory experience, and is independent of the PDE neuron, olfactory function and gentle touch neurons.

MEC-10 and other mechanosensory channels mediate isolation-induced behavioral plasticity before adulthood

To study the genetic mechanisms behind the nociceptive response plasticity, we performed a candidate gene screen for DEG/ENaCs and TRP channels that are expressed in the PVD, where degenerins mediate mechanosensation and proprioception, while TRPs sense low temperatures. In all these signal transduction pathways some of the outcomes are behavioral responses (Chatzigeorgiou et al., 2010, Huang and Chalfie, 1994). We found that the WT-like isolation-induced reduction in harsh touch response was also present in *degt-1* DEG/ENaC and *gtl-1* TRP channel mutants, suggesting that these channels are not directly involved in behavioral plasticity following isolation (Figure 1E). In contrast, for *del-1*, *asic-1* and *mec-10* DEG/ENaC mutants the difference between isolated and crowded conditions was undetectable,

indicating that they are required for such behavioral plasticity. Interestingly, while the harsh touch response of *asic-1* mutants was consistently high, and similar to crowded WT worms, the response for *mec-10* mutants was consistently low, similar to isolated WT animals, regardless of sensory experience (Figure 1E). To test whether the response to harsh touch is dependent on DEG/ENaC activity, we used the DEG/ENaC blocker amiloride (Ben-Shahar, 2011, Bianchi and Driscoll, 2002) on WT worms that were grown in crowded plates. We found that the response to harsh touch was not affected by continuous growth in the presence of amiloride (Figure 1–figure supplement 1C). This result possibly supports the idea that different amiloride-sensitive epithelial sodium channels may have positive and negative effects on the response to harsh touch, which are masked by global inhibition (Figure 1E). This is further evident by the plasticity consequences of some double and triple DEG/ENaC mutant combinations, which are difficult to align into a coherent and simple epistatic genetic model (Figure 4–figure supplement 1).

The DEG/ENaC MEC-10 is expressed in the PVD and responds to mechanosensory signals (Chatzigeorgiou et al., 2010) including shear forces when expressed in heterologous cells (Shi et al., 2016, Shi, Mutchler et al., 2018). Since crowded *mec-10* mutants seem isolated-like in their behavioral response (Figure 1E), we asked how *mec-10* mediates the behavioral plasticity in crowded conditions. To test whether the activity of MEC-10 is required cell-autonomously in the PVD, we expressed MEC-10 under a PVD-specific promoter in a *mec-10* mutant background (Oren-Suissa et al., 2010, Tsalik et al., 2003). We found that expression of MEC-10 in the PVD rescues the low response to harsh touch in crowded *mec-10* mutants, indicating that it acts cell autonomously to modulate behavioral plasticity (Figure 1F).

To determine whether isolation affects the response to harsh touch during development or in adults, we isolated crowded-raised young adults for 24 h and found no difference in their response to harsh touch (Figure 1G). Thus, isolation-induced reduction in mechanosensation is determined before early adulthood, is PVD cell-autonomous, and *mec-10*-dependent.

Experience affects PVD morphology via *mec-10* in adulthood

Altered sensory experience (such as stimuli deprivation) is known to drive synaptic plasticity in the nervous system (Alvarez and Sabatini, 2007, Fox and Wong, 2005, Zuo et al., 2005). However, little is known about the effects of mechanosensory deprivation on the architecture of sensory neurons. To study whether reduced mechanosensory experience can alter the dendritic structure of the PVD we followed the isolated growth paradigm (Figure 1B) and examined two morphological features of the PVD (Figure 2A): The fraction of ectopic (excessive, disordered) branches out of non-ectopic branches (those that form the 'ideal' candelabrum), and the percentage of straight 4th order (quaternary) branches, which form the terminal processes of the candelabrum.

When quantifying the branching pattern of the PVD in adulthood, WT (or WT-like *him-5* background) animals which were isolated as embryos showed an increase in ectopic branching compared with crowded age-matched worms (Figure 2B) and the quaternary branches assumed a more rippled shape (fewer straight 4ry branches, Figure 2C), regardless of the neuron marker utilized (see Figure 2–figure supplement 1).

To determine whether chemical stimulation plays a role in the observed morphological plasticity, animals were isolated onto pheromone-conditioned plates (Maures et al., 2014). Similarly to the response to harsh touch (Figure 1D), chemical stimulation of the plates did not rescue the isolation-induced increase in ectopic branching or the decrease in straight quaternary branches (Figure 2–figure supplement 2). Additionally, we looked at *mec-4* gentle-touch-insensitive mutants (Rose et al., 2005, Suzuki et al., 2003) and found that isolation caused a similar change to PVD structure as in the WT (Figure 2–figure supplement 3, compare with Figure 2B and 2C). In summary, these results suggest that mechanosensory experience controls morphological plasticity of PVD dendritic trees independently of *mec-4* and chemical stimulation.

We next sought to determine whether DEG/ENaCs mediate these experience-driven morphological alterations, by examining PVD morphology in crowded and isolated *mec-10* mutants. We found that crowded *mec-10* animals were different from WT crowded worms, and appear more isolated-like in terms of morphological features (more ectopic branches and fewer straight quaternary branches, compared to crowded *him-5* control animals; Figure 2B and 2C). These results suggest that PVD dendritic morphology is affected by sensory experience in a *mec-10*-dependent pathway. Importantly, these results confirm a role for the mechanosensory channel MEC-10, but not other degenerins (such as ASIC-1), in the plasticity of both the dendritic structure and the nociceptive function of the PVD in the crowded background.

To study whether *mec-10* acts cell autonomously to mediate morphological plasticity, we again utilized PVD-specific MEC-10 expression in a crowded *mec-10* mutant background and found it reduced the fraction of ectopic branches and increased the percentage of straight quaternary branches, compared to age-matched non-transgenic animals (Figure 2D-I). Thus, MEC-10 acts in the PVD to mediate morphological plasticity.

Having identified an isolation-induced morphological plasticity in adults (observed at 72 h from embryo), we next sought to establish the temporal dependence of this effect, by comparing animals after only 48 h, as young adults (see Figure 2–figure supplement 4A). Isolated worms showed a small but significant difference for the percentage of straight quaternary branches, but not in ectopic branching (Figure 2–figure supplement 4B-E) when compared with age-matched crowded worms, suggesting that isolation induces some morphological alterations during

morphogenesis, while some relate to adult-stage maintenance of the neuron. We then isolated animals grown for 48 h in crowded conditions, and found that isolation of young crowded adults for 24 h induced changes in both measured parameters (Figure 2–figure supplement 4F-I), recapitulating isolation of embryos (Figure 2B-C). Thus, isolation of adults for 24 h is sufficient to affect PVD dendritic tree architecture, in contrast to the developmentally-established behavioral response (Figure 1G).

To further determine whether the morphological effect on PVD structure is solely mediated by mechanical cues, we used glass beads under isolated conditions. We found that while the presence of glass beads did not reduce the fraction of ectopic branching, it significantly increased the number of straight quaternary branches (compared with isolated animals without beads, Figure 2J-K). Thus, the mechanosensory stimuli of inert beads can partially rescue isolation-induced morphological changes to the PVD.

Isolation triggers dynamic plasticity of the dendritic tree

To pinpoint the precise time interval required to mediate dendritic arborization changes in adulthood, we examined the effect of varying isolation times on the PVD morphology of crowded-raised young adults. We found that isolation of adults for 2 h had no significant consequence on the structure of the PVD, while isolation of adults for 5 h or longer significantly increased the proportion of ectopic branches and reduced the percentage of quaternary straight branches compared to crowded worms (Figure 3A-B).

To further study plasticity at the individual level, we compared the dendritic tree of individual worms grown under crowded conditions before and after 4 h isolation. This revealed isolation induced more events of ectopic branch growth and fewer events of branch retraction (Figure 3C). Furthermore, this period was sufficient to induce an increase in ectopic branching and a decrease in percentage of straight quaternary branches (Figures 3D, E, and Figure 3–figure supplement 1). Thus, 4 h of isolation are sufficient to induce changes in the architecture of the adult PVD.

Since the geometry of quaternary branches shows rapid response to the amount of mechanosensory stimulation (Figure 3A-E), we next asked how dynamic is this experience-dependent morphological change. We performed a 3 h time lapse imaging in crowded and isolated animals anesthetized with 1% tricaine (Videos 1 and 2). We found that while the number of straight quaternary branches in the isolated worms remained low and stable (~8%), for the crowded animals, we observed a gradual reduction in straight quaternary branches, starting after ~2 h of isolation of individual worms on the slide (Figure 3F,G).

In summary, isolation-induced morphological plasticity is apparent within 2-3 h from the switch from crowded conditions to growth in the absence of mechanical stimuli. This dynamic process involves simultaneous increase in ectopic branching and decrease in straight terminal branches.

Activity affects morphology

It has been shown that activity and sodium influx via the DEG/ENaC UNC-8 promotes synapse elimination in *C. elegans* (Miller-Fleming et al., 2016). To test how global inhibition of DEG/ENaCs affects the morphology of the PVD neuron, we evaluated crowded worms that were grown on plates with amiloride compared to control worms. We found that blocking DEG/ENaCs by amiloride increased the fraction of ectopic branching and decreased the percentage of straight quaternary branches (Figure 3–figure supplement 2A-D). Thus, unlike harsh touch response, which is independent of sensory-level global inhibition (Figure 1–figure supplement 1C), global inhibition at the sensory level alters dendritic morphology. These results suggest that activity via degenerins modulates the structure of the PVD.

To test whether manipulations of other neuromodulators can affect the branching dynamics of the PVD, we utilized two anesthetics: tetramisole, which activates the nematode nicotinic acetylcholine receptors inducing muscle contraction (Aceves et al., 1970), and tricaine, which modulates neuronal activity by blocking sodium channels (Katz et al., 2020), and analyzed their effects during 2-3 h of time lapse movies of crowded and isolated animals. We first tested the commonly used mixture of 0.1% tricaine and 0.01% tetramisole (the racemic mixture of the enantiomer levamisole) (Kravtsov et al., 2017) and found that it induces more growth than retraction of ectopic branches in crowded animals (Figure 3–figure supplement 2E-G). In contrast, 1% tricaine alone has the opposite effect- more retractions of ectopic branches (Figure 3–figure supplement 2H-I; Videos 1 and 2). In addition, 1% tricaine induces more growth for isolated compared to crowded worms, indicating that there are activity-dependent intrinsic factors that are different for the two experience states. These results suggest that modulating neuronal activity triggers structural modifications in the PVD, indicating a possible structural sensitivity to the amount of neuronal activity. In summary, we found that mechanosensory experience, DEG/ENaC protein presence and activity, and pharmacological targeting of activity dynamically affect the structure of the PVD.

PVD structure and function are independent

After establishing that mechanosensory experience induces both a behavioral and a structural plasticity of the PVD, we asked whether there is a causal link between the morphology of the dendritic tree of the PVD and its function as a nociceptor (Hall and Treinin, 2011). We followed the isolation protocol described in Figure 1B for seven combinations of DEG/ENaC mutants and analyzed their response to harsh touch (Figure 4–figure supplement 1) and their PVD structure (Figure 4–figure supplement 2). In order to compare the morphological properties of the different DEG/ENaC genotypes under different sensory experience (crowded, isolated; Figure 4–figure supplement 2), we used discriminant analysis. This provides a supervised classification method to

combine all the analyzed morphological phenotypes, including loss of self-avoidance between adjacent candelabra (Figure 4–figure supplement 3), into a certain value characterizing the PVD morphological state (Figure 4A). We then superimposed the behavioral results of the DEG/ENaC mutants' response to harsh touch (Figure 4–figure supplement 1) on the morphological clustering, as a binary-like property (<45% responding for isolated WT versus >65% for crowded WT, as shown in Figure 4–figure supplement 1*)*. We found no correlation between the morphology of the PVD and the response to harsh touch when testing the different combinations of genotypes and treatments. For example, isolated *mec-10; degt-1* double mutants show crowded-like morphology with isolated-like behavioral response (Figure 4A and Figure 4–figure supplement 1 and 2). These findings suggest that while degenerins are required for isolation-induced plasticity of both traits, response to harsh touch is independent of the structural alteration of the PVD.

An additional line of evidence supporting the independence of the behavioral and morphological phenotypes was demonstrated by isolation of young adult worms for 24 h (Figure 3). This isolation affects the structure of the PVD (Figure 2–figure supplement 4) but has no effect on the response to harsh touch (Figure 1G). Amiloride also has no effect on harsh touch response (Figure 1–figure supplement 1C) but does alter dendritic morphology (Figure 3–figure supplement 2A-D). Finally, to directly demonstrate that these two features are independent, we assayed harsh touch responses of isolated animals and then analyzed each individual animal for its PVD morphology. We then compared the dendritic morphology of responding and non-responding worms, and found that the morphological parameters were similar (Figure 4B-E). Thus, analysis at the level of individual worms failed to demonstrate a correlation between the morphology and the response to harsh touch. In summary, the morphological and behavioral phenotypes were independently affected by sensory experience via degenerins. We cannot exclude the possibility that other functions of the PVD, like the response to low temperatures (Chatzigeorgiou et al., 2010) and proprioception (Albeg et al., 2011) are more tightly associated to the structure of the PVD, nor that the morphological changes induced by isolation are too minor to constitute a difference in neuronal function.

In addition to the isolation-induced changes in the number of ectopic branches and the percentage of straight quaternary branches, we found that worms raised in isolation are also more likely to lose the self-avoidance between two adjacent menorahs (candelabra). This effect is also *mec-10*-dependent, but appears to act cell non-autonomously. In addition, it is chemosensory and amiloride independent (Figure 4–figure supplement 3).

MEC-10 and DEGT-1 localization is experience-dependent

Differential localization of degenerins can affect both the behavioral response to harsh touch and the structural properties of the neuron. When considering the effect of

isolation, we hypothesized that changes in the localization patterns of DEG/ENaC can account for plasticity at both the behavioral (Figure 1) and the structural level (Figure 2). Since MEC-10 and DEGT-1 tend to co-localize within the PVD (Chatzigeorgiou et al., 2010) we analyzed the interaction between these two proteins, under different mechanosensory experiences. We found that MEC-10 localization in the plasma membrane, in intracellular vesicular compartments of the axon and in the quaternary branches was reduced after isolation (Figure 5A-D, Videos 3 and 4). In contrast to MEC-10 (Figure 5A-D), DEGT-1 localization is reduced only in the cell body following isolation (Figure 5E-H). Furthermore, *degt-1* mutants show reduced MEC-10 signal, and more importantly, abrogated the isolation-induced reduction in MEC-10 localization at the quaternary branches and the axon (Figure 5A-D). In the reciprocal experiment, DEGT-1 localization was affected in *mec-10* mutants, as isolated worms exhibit increased localization to the cell body compared with WT isolated worms (Figure 5E-H). Thus, mechanosensory experience also induces plasticity in the localization pattern of MEC-10 and DEGT-1. We propose this differential localization may be part of the mechanism that independently and locally modulates dendritic and axonal properties, to affect both the structure and the function of the PVD, respectively.

Optogenetic stimulation suggests behavioral plasticity is post-sensory

We have shown that sensory deprivation (isolation) affects the localization of two different mechanoreceptors, the degenerins MEC-10 and DEGT-1, in the dendrites, axon and soma of the PVD. It is conceivable that the differential localization of degenerins in different domains of the PVD may affect the morphology and function of the PVD. Thus, we decided to activate the PVD independently of the endogenous mechanoreceptors and study whether the escape behavior is similar in isolated and crowded animals. We hypothesized that if we circumvent the normal degenerin-mediated mechano-stimulation, exciting the PVD downstream to sensory activity, the animals grown in isolation will respond to the same degree as if they were in crowded conditions and independently of the dendritic tree morphology. Thus, we used optogenetic stimulation with Channelrhodopsin (ChR2) expressed in the PVD (Husson et al., 2012) to activate the neuron while bypassing sensory perception. We found that isolation significantly reduced the percentage of worms responding to optogenetic stimulation of the PVD (Figure 5I), indicating that the plasticity in the response is acting downstream to PVD activation, mechanosensory channels and signal transduction pathways. This activation is sensitive to isolation probably because it is acting pre- or post-synaptically.

To determine whether optogenetic stimulation of isolated animals can reverse the morphological changes induced by the absence of mechanical stimuli in PVD, we used optogenetic stimulation of the PVD and found no significant difference between isolated and isolated optogenetically-stimulated animals in any of the measured PVD structural characteristic (Figure 5–figure supplement 1). Thus, optogenetic stimulation on isolated

animals is not sufficient to convert their dendritic trees to crowded-like. In addition, the reduced response of isolated animals to optogenetic stimulation suggests the escape response is not dependent on the structure of dendritic trees but on unknown downstream pathways.

Calcium dynamics in response to harsh touch are similar in isolated and crowded animals

Having shown that PVD optogenetic activation elicits a weaker escape response in isolated animals, we asked whether this occurs at the level of PVD itself, or originates further downstream.

To determine whether spontaneous Ca^{++} dynamics in PVD is different between crowded and isolated animals we first observed the baseline calcium dynamics in animals grown isolated and crowded. We found no significant differences in the calcium levels between the isolated and crowded animals (Figure 6–figure supplement 1). To directly elicit PVD mechanosensory activation in isolated and crowded animals, we performed calcium recordings under mechanical stimuli using a custom microfluidic device (Nekimken et. al., 2017). The device allows for the controlled application of mechanical stimulation, and was previously applied to study gentle-touch receptor neurons (TRNs) (Sanfeliu et al., 2023) and AVG (Setty et al., 2022). Similar devices were used for PVD (Cho et al., 2017; Tao et al., 2019). To emulate harsh touch using our device, a 3 bar pressure caused a 15 µm cuticle displacement, greater than the indentation used for studying TRNs and similar to the tail stimulation paradigm used by Setty and colleagues (Setty et al., 2022). Previously we have shown that TRNs responded most efficiently to a high frequency stimulation but were largely insensitive to stimuli delivered below 2 Hz (Nekimken et. al., 2017). We applied three different stimulus profiles: a single step indentation (‘step’), similar to a brief manual harsh-touch prod, as well as a gradual pressure ‘ramp’ increase (‘sawtooth’; in which the pressure increases slowly to 3 bar within 2s) and a 10 Hz ‘buzz’ vibration (see Materials and Methods). Even though we observed a strong and robust activation of PVD for all three stimuli tested (Figure 6), the response to the ‘sawtooth’ was significantly weaker (Figure 6A). Moreover, we noticed that the response correlated with the abrupt offset of the force in the ‘saw tooth’, rather than the gradual onset (Figure 6Aiii). To corroborate this result, we also tested a 20 s square step, and indeed found a separate response at the onset as well as the offset (Figure 6–figure supplement 2, Video 7). Thus, PVD, like TRNs, responds better to faster strain rates and adapt under continuous deformation (Eastwood et al., 2015). Using this analysis, we found that both isolated and crowded animals responded similarly and efficiently across all three types of stimuli (Figure 6, Videos 5, 6). Together, these results suggest that the difference in the behavioral response to external mechanical stimuli is due to a pre and/or postsynaptic effect

following mechanosensory deprivation and not a direct consequence of the morphological changes in the structure of the PVD or its intrinsic activity at the level of the cell body.

In summary, our genetic and pharmacological evidence suggest that dendritic structural plasticity is an autonomous activity-dependent homeostatic mechanism. Combined with optogenetic testing and calcium imaging for mechanically stimulated PVD, our results indicate that dendritic tree plasticity is independent from downstream processes that affect escape behavior in response to harsh touch.

Discussion

From the evolutionary point of view, dendritic trees, their morphogenesis (Heiman and Bülow, 2024) and their structural complexity remain mysterious objects, despite many efforts to understand the contribution of arborization complexity to dendritic physiology and function (Hausser and Mel, 2003).

Previous research has demonstrated both cell autonomous (Aguirre-Chen et al., 2011, Oren-Suissa et al., 2010, Salzberg et al., 2014) and cell non-autonomous (Dong et al., 2013, Salzberg et al., 2013) mechanisms that regulate the PVD's dendritic morphogenesis during development. Some studies have also focused on regeneration and aging effects on the tree structure of the PVD, revealing plasticity in the adult stage (Iosilevskii and Podbilewicz, 2021, Kravtsov et al., 2017, Oren-Suissa et al., 2017), similar to what has been shown for *Drosophila* sensory neurons (DeVault et al., 2018). We found, by using mutants for DEG/ENaCs, chemosensory stimulation, pharmacology, optogenetic stimulation and glass beads, that the dendritic structure of the PVD and the behavioral response to harsh touch are activity- and mechanosensory-dependent, but appear to be chemosensory-independent. It is still conceivable that chemosensation can affect nociception and proprioception, in a cross modal plasticity mechanism, but at the moment we do not have evidence for this scenario. In contrast, we show that DEG/ENaCs mechanosensory channels (degenerins) affect the architecture of the PVD.

Our results suggest that 'nurture', manifested as mechanosensory experience, activates mechanotransduction signaling, via DEG/ENaCs amiloride-sensitive activity, to stabilize the homeostatic structure of the dendritic tree in adults. The sensory experience induced when one body side of the worm is in contact with the agar plate is not sufficient for this purpose (Figure 7–figure supplement 1); however, other worms on the plate, or the presence of glass beads, elicit significant structural alterations. Moreover, the cell autonomous activity of MEC-10 in the PVD was found to be both necessary and sufficient to preserve the crowded-experience phenotype in terms of the simplified structure of the PVD. While there are other multiple plausible explanations, our failure in remodeling the isolated-state arbor by repeated optogenetic activation of the PVD may provide further evidence for the necessity of DEG/ENaCs in this structural plasticity, since neuron activation by ChR2 bypasses the activation of mechanically-

gated DEG/ENaC channels. Figure 7 depicts our working model, where the amount of mechanosensory stimulation, in crowded or isolated conditions, affects the expression and localization of MEC-10 and DEGT-1 in different compartments of the PVD. Localization of MEC-10, probably by forming higher-order complexes with other DEG/ENaCs, can affect the structure of the PVD at the level of the dendritic tree. The morphological and behavioral phenotypes shown here were rescued by a PVD-specific expression of MEC-10, supporting such a cell autonomous mechanism. The experience-induced structural plasticity seems homeostatic at the individual branch dynamics level in the adult. In contrast, we show that the behavioral response to harsh touch is modulated by mechanosensory experience during development and by the presence of DEG/ENaCs, and perhaps involves other neurons downstream. Based on optogenetic stimulation, we presume that the behavioral plasticity is a pre- and/or post-synaptic property, mediated by DEG/ENaCs (Hill and Ben-Shahar, 2018) and related to neurotransmission modulation, independently of the structure of the PVD dendritic tree. These structural and behavioral plasticity are separated in time (adulthood vs. development) and space (dendrite vs. axon; Figure 7). We found no correlation or causation between the structure and the nociceptive function of the PVD. It is possible that such a link exists, but our physiological and behavioral outputs are not sensitive enough to detect it.

The PVD is a polymodal sensory neuron, and it has been shown that its dendrite structure is related to body posture, while the response to harsh touch is related to synaptic connection (Tao et al., 2019). Current assays for proprioception in *C. elegans* largely rely on video movement tracking, and it is possible the changes in the dendrite structure caused by sensory deprivation are too minor to cause any quantitative changes in body posture. Elegant work by Tao and colleagues (2019) supports the role of MEC-10 in PVD-mediated proprioception, however has some discrepancies with our results with regard to harsh touch response, which may be related to the different methodologies used, as well as to the animals' age and mechanosensory experience (Inberg and Podbilewicz., 2018).

Calcium imaging reveals PVD responds to fast changes in mechanical stress, which includes pressure onset as well as offset (Figs. 6Aiii, Figure 6–figure supplement 2, Video 7). We found PVD to be insensitive to slow stimuli and adapt under constant mechanical body deformation. This adaptation may facilitate the response to a wide dynamic range of stimuli applied to the body wall and is thus an essential feature of mechanical nociception. While TRNs respond to both the application and release of a step stimulus (Eastwood et al., 2015), other mechanosensory channels in different mechanosensitive systems respond preferentially to either on or off instead of a symmetric response to both (Katta et al., 2015). Interestingly, previous calcium imaging studies on PVD have not described the response to offset (Chatzigeorgiou et al., 2010; Husson et al., 2012; Tao et al., 2019; Cho et al., 2017, Cho et al., 2018). One possible

explanation to our new observation may be due to the fact that we are the first to apply 'sawtooth' stimuli to the PVD with a slow increase such that the activity is not induced. An alternative explanation is that in previous work, the onset and offset were too close (e.g. for a 0.5 s step as in Tao et al., 2019), such that the onset and offset could not be differentiated.

Our results indicate that sensory experience does not alter the magnitude of the calcium activation (Figure 6), as tested using three different stimulation profiles. These findings support additional effects downstream to the dendritic structural plasticity, which govern behavioral plasticity and add another layer of support to the separation in time and space between the structure of the PVD and its function.

Somatosensory activation in vertebrates plays a prominent role in shaping the structural and functional properties of dendritic spines, mainly studied in the central nervous system (Gyorffy et al., 2018, Holtmaat and Svoboda, 2009, Xu, Yu et al., 2009, Yang et al., 2009). In contrast to mammalian cortical neurons, much less is known about sensory neurons' degree of plasticity and the molecular mechanisms utilized during adulthood. Here we suggest that degenerins mediate mechanosensation-induced dendritic growth in sensory dendrites. The dendritic plasticity we described bears resemblance to the activity-dependent effect of glutamatergic signaling and NMDA receptors. Activity via NMDA affects dendritic spines as an upstream mechanism of cell signaling, resulting in structural modifications (Nagerl et al., 2004, Star et al., 2002, Stein et al., 2021, Zhang et al., 2015). It is possible that degenerins mediate mechanosensory signaling sensation, by activating cationic gradients (Kellenberger and Schild, 2002), leading to activation of downstream intracellular signaling pathways (Ghiretti et al., 2014, Sin et al., 2002, Vaillant et al., 2002, Zhou et al., 2006), which in turn stabilize local, actin-mediated (Halpain, 2018, Luo, 2002, Zuo et al., 2005) structural plasticity in the PVD dendritic branches. In *Drosophila,* at the epithelium, mechanosensitive ion channels, together with E-cadherin-catenin complexes and calcium sensing mechanisms affect epithelial morphogenesis (Choudhury et al., 2021). In parallel, DEG/ENaCs may also modulate pre- and post-synaptic homeostatic signaling in the harsh touch circuit, as has been shown in neuromuscular junctions (Younger et al., 2013). While this study focuses on degenerins activation in the PVD with emphasis on dendritic structures, future studies may establish the pre- and -post-synaptic mechanisms which act downstream, on the transcriptional and translational levels. These directions for future studies have the potential to increase our understanding of the mechanisms that couple sensory experience, to structural dendritic plasticity.

In summary, we propose that the combinatorial actions of DEG/ENaCs have mechano-signaling functions mediating plasticity in sensory dendritic trees, and provide mechanistic insights into dendritic structural responses to sensory experience in adulthood and the behavioral consequences of such adaptations during development.

Materials and Methods

Strains

Nematode strains were maintained according to standard protocols (Brenner, 1974). The list of the strains is presented in Supplementary file 1a. Strains of the DEG/ENaCs family obtained from the CGC (JPS282: *asic-1*(*ok415*) I, ZB2551: *mec-10*(*tm1552*) X, VC2633: *degt-1*(*ok3307*) V) were crossed with BP709: *hmnIs133[ser-2Prom3::kaede]*. The validation of F2 homozygotes for the DEG/ENaCs deletions (including single, double and triple mutants) was performed by PCR amplification of the genomic area containing the deleted region.

Primers for Multiplex PCR

The list of the primers used is presented in Supplementary file 1b.

Spinning disk confocal microscopy

Prior to imaging, the worms were mounted on a 10% agar pad placed on a microscope glass slide, in 1 µl polystyrene bead suspension (100 nm diameter; Polysciences, Inc.) for their mechanical restraint, and sealed with a coverslip for complete physical immobilization (Kim et al., 2013). The PVD neuron was visualized using a Yokagawa CSU-X1 spinning disk, Nikon eclipse Ti inverted microscope and iXon3 camera (ANDOR). Images were captured with MetaMorph, version 7.8.1.0. For each worm, a sequential z-series image stack (step size of 0.35 µm) was obtained with an oil Plan Fluor 40X (NA 1.3) lens around the PVD cell body, encompassing approximately 50-100 µm segments both anteriorly and posteriorly.

Data analysis

The analysis of the PVD structure was performed for the area surrounding the cell body. All images were analysed with ImageJ, version 1.48 (NIH), in TIFF format, by producing a maximal intensity z-series projection and converting it to negative form (invert lookup table) for improved visibility. Ectopic branching was defined as described previously (Hausser and Mel, 2003). Briefly, non-ectopic branches form the ‘ideal’ WT candelabrum of the late L4 stage, whereas excess branches, which create non-quaternary terminal ends, are considered ectopic, as illustrated with dashed lines for ectopic branching in Figure 2A. The total number of ectopic and non-ectopic branches was quantified for each image, and presented as a fraction (ectopic/non-ectopic branches).

The geometry of each quaternary branch was defined in the following manner: Straight geometry- all the pixels that constitute the branch are positioned on a straight line generated with ImageJ. The width of the line (1 pixel) was constant for the entire sets of experiments. The number of straight quaternary branches were divided by the total quaternary branches in the image for each worm and presented as a percentage. The analysis was done only for worms which did not move through the Z series. Moving

worms were excluded from the experiment. Self-avoidance defects- the number of events where two adjacent candelabra overlapped (no gap formation), was divided by the total number of gaps between the candelabra within the frame (Figure 2A, Figure 4 – figure supplement 3). The self-avoidance values are presented as percentage.

Behavioral procedures

Harsh touch assay

After 72 h, adult worms (both isolated and those from the crowded plate as described below) were transferred using an eyelash each to a new agar plate, freshly seeded with 150 µl OP50 (about 16 h after seeding). This step is required to avoid a thick edge of the bacterial lawn, which might interfere with harsh touch response measurement. After ~45 minutes in the plate, the non-moving worms were prodded with a platinum wire posterior to the vulva, above the interface between worm's body and the agar plate (Way and Chalfie, 1988), every 10 seconds, and the number of responses to harsh touch was counted. Animals with a functional PVD moved, sometimes backing up. More than one response constitutes a responsive animal. The non-responding worms were defined if two prodding events were observed sequentially without response. The percentage of responding worms was calculated for each genotype and treatment. The experimenter was blind to both the genotype and the treatment- crowded or isolated.

Isolation of embryos

To establish the method for conspecifics based mechanosensory stimulation, we performed several calibration experiments with different population densities (250 embryos, progeny of 15 adults, progeny of 30 adults) to test conditions for the crowded plate.

We found a gradual increase in the crowding effect and reduced variation in the measured parameter. Following that, we decided to work with the progeny of 30 crowded adults as a source of mechanosensory signal.

The worm isolation procedure was based on previous work (Rose et al., 2005) with a few modifications, as indicated. Isolated animals were grown on 6 cm agar plate with 150 µl of OP50 *E. coli*, while crowded plate worms were grown on 600-700 µl OP50 to prevent starvation. The embryos and adult worms were isolated with platinum wire. The plates were sealed with one layer of Parafilm M and placed into a plastic box, at 20 ºC, for the entire experiment.

Three experimental groups were used for the 72 h (96 h of experiment was performed only for *mec-4* worms, since they were L4- very young adults at 72 h) isolation experiment: **(1)** Single isolated embryos **(2)** Crowded worms - the progeny of 30 young, non-starved, adults (approximately, 7,000-9,000 worms in different developmental stages, without approaching starvation) **(3)** Crowded adult worms that were isolated for a certain amount of time as adults.

After 48/72/96 h (according to the experiment), age-matched worms from each group were transferred to 10% agar pad slides for imaging, as described above (Spinning disk confocal microscopy) (Rose et al., 2005).

Isolation of adults for 2, 5, 15 or 24 hours

Crowded plates were prepared as described above, with progeny from 30 adult hermaphrodites. Animals were separated into individual plates for the desired time window before 72 h have passed (*i.e.* after ~70 h for 2 h isolation, ~67 h for 5 h isolation etc.). Worms were isolated using an eyelash into new plates containing 150 µl of OP50. At 72 h, the PVD of isolated animals was imaged and compared with age-matched animals which remained in the crowded plate of origin (see Figure 1B).

Optogenetics stimulation for harsh touch

Crowded and isolated worms (ZX819: *lite-1(ce314) X; zxIs12[pF49H12.4::ChR2::mCherry pF49H12.4::GFP*]) were grown on OP50 with 100 µM All Trans Retinal (ATR, Sigma R2500), in order to obtain functional Channelrhodopsin (Husson et al., 2012) (as a control we tested the response of worms that were grown on ethanol alone, no response was detected for these worms). After 72 h the worms were singly mounted with eyelash on a chunk (1 cm X 1 cm) of agar that was mounted on a microscope glass slide. The agar contained fresh but dry OP50, with 100 µM ATR. About 30 minutes following the transfer the worms were tested for the response to light. Worms were stimulated at 488 nm wavelength, with laser intensity of 40% and exposure time of 100 ms, with 10X Plan Fluor (NA 0.3) for ~1 second and the forward acceleration response was measured. The microscope system is as described above. The experimenter determined the presence or the absence of forward acceleration in response to light activation.

Optogenetics stimulation of isolated worms

Isolated eggs were grown as described at the 'Isolation of embryos' section. Isolated worms (ZX819: *lite-1(ce314) X; zxIs12[pF49H12.4::ChR2::mCherry pF49H12.4::GFP*]) were grown on 150 µM OP50 with 100 µM ATR (Husson et al., 2012) or 0.3% ethanol as control. After 72 h both the crowded and isolated worms were singly mounted with eyelash onto a cube (with surface area of about approx.1 cm^2, depth of 0.5 cm) of agar layered with fresh, fully dried, OP50 with 100 µM ATR or 0.3% ethanol as a control group. The worms were stimulated with 488 nm wavelength, with laser intensity of 40% and exposure time of 100 ms, with 10X Plan Fluor (NA 0.3) for ~60 seconds, every 5 min during 4 h. Stimulation and recording was performed with the microscope system described above.

As a control, before each experiment, crowded ZX819 worms were tested for forward acceleration as a positive control to the functionality of the ChR2. After the end of 4 h stimulation, the worms were mounted for imaging of the PVD at 40X as described under "Spinning disk confocal microscopy" section.

Isolation with chemical stimulation

The *glp-4(bn2)* mutants which are sterile at 25°C were used (~40 worms for each plate), in order to prepare conditioned/chemically stimulated plates (Maures et al., 2014) prior to growing isolated animals. The *glp-4* mutants were transferred at early larval stage (L1, L2) to a new agar plate for 96 h at 25°C. After the removal of the *glp-4* mutants, the embryo isolation procedure was used, as described before at 20°C.

Isolation with glass beads

Single embryos were isolated to agar plates with 150 µl OP50 and 2.5 g of glass beads (1 mm diameter) were placed on the OP50 lawn in the middle of the plate. The worms were isolated for 72 h and tested for response to harsh touch as described above.

Pharmacology

Amiloride hydrochloride hydrate (Sigma, #A7410) 1 M stock solution in DMSO was stored at -20°C. A final concentration of 3 mM amiloride in 0.03% DMSO was prepared in OP50 bacteria (LB medium) and seeded on NGM plates. 650 µl of the OP50 mixture was seeded on each plate. As a control, 0.03% DMSO was added to OP50 bacteria. For each plate (control 0.03% DMSO or 3 mM amiloride) 30 non-starved adult worms were added. After 72 h at 20°C the progeny of the 30 adults were tested as young adults for their PVD morphology and their response to posterior harsh touch, as described in the previous sections.

Anesthetics and long-term imaging

In addition to immobilization of worms with 100 nm polystyrene beads as described in the ”Spinning disk confocal microscopy” section above, two additional methods for long term imaging and pharmacological effects assays were used: 1% tricaine (Sigma, A5040) in M9 buffer or a mixture of 0.01% tetramisole (Sigma, T-1512) and 0.1% tricaine in M9 buffer were utilized.

Worms were exposed to the anesthetics (in a glass well) for ~20 min until paralyzed, then transferred to 3% agar pads with 1 µl of the anesthetics. Sequential z-axis image series (0.6 µm step-size) were taken, as described above, every 5 min for 2-3 h.

Imaging individual worms- crowded to isolated

Worms were grown at crowded conditions, as described above. At ~24 h of adulthood, individual worms were placed in a 1% tricaine solution in M9 buffer for 10 min until paralyzed and transferred to 3% agar slides with 1 µl 1% tricaine. Following a short PVD imaging session, the worms were recovered from the slide with M9 and isolated to a new plate for 4 h. Each 4 h-isolated animal was anesthetized once again with 1% tricaine for 10 min prior to PVD imaging.

Analysis of DEG/ENaCs localization in the PVD

Two DEG**/**ENaCs protein constructs, *pF49H12.4*::MEC-10::mCherry and *pF49H12.4::DEGT-1*::mCherry (plasmids kindly provided by W. Schafer’s lab, (Chatzigeorgiou et al., 2010)) were analysed for their localization in the PVD, by

comparing worms expressing the co-injection marker *punc-122*::GFP raised in crowded or isolated conditions, in a similar behavioral assay as described in Figure 1B. A z-series (step size of 0.35 µm, immobilization performed with polystyrene beads, as described in the microscopy section) of the area around the cell body of the PVD was obtained with a 60X Apochromat (NA 1.4) lens. The images (after maximal intensity projection of the Z-series) were encoded so the analysis was performed in a blind manner. The presence or absence of fluorescent signal was examined in three compartments: The cell body, the quaternary branches and the axon of the PVD.

Rescue strains

Worms from BP1022 (*mec-10(tm1552) X*; *hmnIs133[ser-2Prom3::Kaede]*; *him-5(e1490) V*) were injected into the gonad with a rescuing plasmid for *mec-10*, with a PVD specific promoter (pWRS825: *ser-2Prom3::mec-10* genomic) kindly provided by W. Schafer's lab (Chatzigeorgiou et al., 2010). The injection mix contained *myo-2p::GFP* (20 ng/µl) as a co-transformation marker and pWRS825 (80 ng/µl). For both behavioral and structural characterization, the *him-5; mec-10* strain, with and without rescuing plasmid, shared the same crowded plate and were differentiated by the presence or absence of the co-injection marker.

Effect of plate on PVD in contact with agar and the opposing side

Embryos were singled into plates with 150 µl OP50 bacteria at 20°C, and analyzed as young adults 72 h later. Every animal was transferred using an eyelash into freshly seeded plates (<24 h), and noted for its side orientation. Once on these experiment plates, animals were observed for their side orientation at 30-minute intervals for a minimum of 3 h prior to microscopy.
For microscopy of both PVD neurites, while few animals were removed from the slide and repositioned using an eyelash, most animals were imaged using a coverslip 'sandwich' method (adapted from (Sulston et al., 1983)), whereby the animal is pressed on an agar pad between two large coverslips, which are subsequently flipped as a single unit and observed from the other side. Briefly, a thin 3% agar pad was pressed onto a 24x50 mm coverslip (170±5 µm thick), placed on a standard microscope slide for ease of handling. Animals were singly placed in a drop of 0.05% tetramisole (Sigma, T-1512) in M9 on the agar pad using an eyelash, and a second, similar coverslip was immediately placed above. The two coverslips were sealed shut onto the supporting slide using two thin strips of marking tape, and once the animal was immobilized the PVD on the side closest to the objective was imaged as described above (see Spinning Disk confocal microscopy). For viewing the opposite neurite, the tape was carefully peeled and the two coverslips flipped as one, taped again, and similarly imaged. Note that this method inevitably makes the second side imaged to be fainter due to the laser penetrating through the agar pad layer itself; laser intensities were typically increased by up to 5% in order to compensate for the decrease in fluorescence.

Micromechanical experiments and calcium image recordings

Micromechanical experiments were performed in microfluidic devices which have been prepared as described using a 15:1 PDMS base-polymer/curing agent ratio (Fehlauer et al., 2018; Setty et al., 2022), by replicating a design presented in (Nekimken et. al., 2017). Prior to the experiments, single animals raised in isolated conditions or multiple animals raised in the crowded conditions were loaded into the device as described (Fehlauer et al., 2018). After gently pushing individual animals into the trapping channel, a sequence of three different stimulus profiles (2 s each, 3 bar max pressure, immediate 'step', sawtooth (or gradual 'ramp') or 10 Hz vibration `buzz') were applied (Nekimken, et. al., 2017) each separated by 20 s. The pressure-deformation relation was previously characterized (Setty et al., 2022). Accordingly, we found a deformation of 15 µm with a 3 bar pressure on the channel. In all cases, the animals ended up with the lateral sides facing the side walls of the chip, providing a ventral or dorsal view of the body. Stimuli location was within 200 µm of the PVD cell body (either anterior or posterior), and ipsilateral or contralateral.

Imaging was performed using a 40x (NA1.1) water immersion lens on an inverted Leica DMi8 equipped with a Hamamatsu Orca Flash 4 camera, and a fluorescence cube with a multiband dichroic mirror (Semrock Quadband FF409/493/573/652). Calcium sensitive and insensitive channel were divided into its spectral components using a Hamamatsu Gemini W-View beamsplitter with a 538 nm edge dichroic (Semrock, FF528-FDi1-25-36) and projected on either half of the camera chip. A Lumencor Spectra X LED light source (using the cyan-488 and green-555 LED) was used to excite the Ca-sensitive and insensitive dye, respectively, and slaved to the camera acquisition with an exposure time of 100 ms in HCImage Software (version 4.4.2.7). Likewise, the pressure application (ElveFlow OB1 with an 8 bar channel) was synchronized to the camera acquisition using the SMA trigger out, with a delay equal to the pre-stimulus period.

The whole procedure including loading, focusing, and stimulation did not take longer than 5-10 min per animals to avoid pre-stimulus adaptation. All animals remained viable after the procedure, as visualized by vivid and lively thrashing in the buffer.

Analysis of calcium traces after stimulation

All quantifications were performed on the PVD cell body after ipsilateral application of the mechanical stimulus. No dependence of the calcium signals on the anterior/posterior position was noticed. Contralaterally applied stimuli lead to a strongly reduced response, without detectable difference between the two conditions (isolated, crowded), but were not further analyzed. To extract calcium signals from the cell body, a procedure described in (Porta-de-la-Riva et al, 2023) was followed. Calcium traces were

background subtracted, baseline corrected, and normalized by the first 10 s preceding the first mechanical stimulus. Results are displayed as fold change, compared to baseline calcium levels.

PVD basal activity

To image spontaneous calcium traces in PVD, we used worms that were raised in isolated or crowded conditions, as described above. Using a drop of S-basal buffer, adult worms were inserted in a dual olfactory chip (Gat et al, 2023; Karimi et al, 2024), with a flow rate of 0.005 ml/min. Imaging was done with a Zeiss LSM 880 confocal microscope using a 40x magnification water objective. When the worm was properly located inside the chip with minimal movement, PVD was imaged for 1:30 minutes, with imaging rate of 6.667 Hz.
For analysis, the GCaMP6s fluorescence intensity was measured using FIJI. ROIs of PVD soma were picked manually to extract mean intensity values. Data analysis was performed using Python 3.10. For each worm, the baseline fluorescent level (F0) was calculated by averaging the mean values of 100 frames in the beginning of each recording. Then, for each frame, ΔF was calculated by subtracting F0 from the value of that time point, and the result was divided by F0, to normalize the differences in the fluorescence baseline levels between individuals (ΔF/F0). For Figure 6–figure supplement 1C, the derivative of ΔF/F0 was calculated and averaged across worms in each time point. Then, a histogram representing the distribution of the average derivative was plotted.

Statistics and data plotting

At least two independent experiments constitute the data set described in each figure. For the morphological characterization of the PVD the results are expressed as means (blue circle) ± standard error of the mean (s.e.m.). In the boxplot (first, third quartiles) the upper whisker extends from the hinge to the highest value that is within 1.5 * IQR (inter-quartile range), the distance between the first and third quartiles. The lower whisker extends from the hinge to the lowest value within 1.5 * IQR of the hinge.
The statistical analyses were performed with SPSS software (IBM, version 20) and “R package”. Two-tailed tests were performed for the entire data sets.
Since for many experiments the distribution of the data was not normal, nonparametric tests were used: Mann-Whitney test for comparison between two independent groups. Kruskal-Wallis test was used for multiple comparisons for more than two groups.
For proportions (percentage worms) ± standard error of proportion was calculated. Fisher’s exact test was used for analysis of differences in proportions. To estimate the variability in proportion we calculated the Standard Error of Proportion: $\sqrt{\frac{(1-p)\cdot p}{n}}$
The dot plot figures were prepared with “R package”, the bar charts with Microsoft Excel software. Final figures were prepared with Adobe Illustrator CS version 11.0.0.

Discriminant analysis

Eight different strains (WT and seven DEG/ENaCs), with two treatments (crowded, isolated worms) for each strain were analyzed for Linear discriminant analysis for morphological characteristics, to evaluate similarity between different strains and treatments. Each worm in the data set was characterized by the three morphological characteristics (the fraction of ectopic branching, the percentage straight quaternary branches and the percentage of self-avoidance defects). The centroid for morphological characterization was calculated for each condition and represented by a square. Data from independent harsh touch experiments are shown for each group. The analysis was performed using SPSS 20.

Acknowledgments

We thank current and former lab members for their intellectual and technical support. Veronika Kravtsov, Sagi Levy, Anna Meledin, Tom Shemesh, Shay Stern, Yehuda Salzberg and Alon Zaslaver for critically reading and commenting on the manuscript. Ehud Ahissar, Dan Cassel, Michel Labouesse and Kang Shen for fruitful discussions. William Schafer, Max Heiman, Hannes Bülow, Yehuda Salzberg and Alexander Gottschalk for plasmids and strains. Some strains were provided by the Caenorhabditis Genetics Center (CGC), which is funded by NIH Office of Research Infrastructure Programs (P40 OD010440). This work was supported by grants from the Israel Science Foundation (442/12 and 257/17, BP), Adelis Fund (2023479, BP), and the Ministry of Science and Technology (3-13022, BP). MK acknowledges PID2021-123812OB-I00 and the CNS2022-135906 project funded by MCIN /AEI /10.13039/501100011033 / FEDER, UE, and the HFSPO through the RGP021/2023.

References

Aceves J, Erlij D, Martinez-Maranon R (1970) The mechanism of the paralysing action of tetramisole on Ascaris somatic muscle. British journal of pharmacology 38: 602-607

Aguirre-Chen C, Bülow HE, Kaprielian Z (2011) C. elegans bicd-1, homolog of the Drosophila dynein accessory factor Bicaudal D, regulates the branching of PVD sensory neuron dendrites. Development 138: 507-18

Albeg A, Smith C, Chatzigeorgiou M, Feitelson DG, Hall DH, Schafer WR, Miller DM, 3rd, Treinin M (2011) C. elegans multi-dendritic sensory neurons: Morphology and function. Mol Cell Neurosci 46: 308-317

Alvarez VA, Sabatini BL (2007) Anatomical and physiological plasticity of dendritic spines. Annual review of neuroscience 30: 79-97

Bailey NW, Moore AJ (2018) Evolutionary Consequences of Social Isolation. Trends in ecology & evolution 33: 595-607

Baldin JP, Barth D, Fronius M (2020) Epithelial Na+ Channel (ENaC) Formed by One or Two Subunits Forms Functional Channels That Respond to Shear Force. Frontiers in Physiology 11

Ben-Shahar Y (2011) Sensory Functions for Degenerin/Epithelial Sodium Channels (DEG/ENaC). Adv Genet 76: 1-26

Bianchi L, Driscoll M (2002) Protons at the gate: DEG/ENaC ion channels help us feel and remember. Neuron 34: 337-340

Brenner S (1974) The genetics of *Caenorhabditis elegans*. Genetics 77: 71-94

Caneo M, Julian V, Byrne AB, Alkema MJ, Calixto A (2019) Diapause induces functional axonal regeneration after necrotic insult in C. elegans. PLoS Genet 15: e1007863

Chalfie M, Sulston J (1981) Developmental genetics of the mechanosensory neurons of Caenorhabditis elegans. Dev Biol 82: 358-370

Chatzigeorgiou M, Yoo S, Watson JD, Lee WH, Spencer WC, Kindt KS, Hwang SW, Miller DM, 3rd, Treinin M, Driscoll M, Schafer WR (2010) Specific roles for DEG/ENaC and TRP channels in touch and thermosensation in C. elegans nociceptors. Nature neuroscience 13: 861-868

Chen Y, Bharill S, Isacoff EY, Chalfie M (2015) Subunit composition of a DEG/ENaC mechanosensory channel of Caenorhabditis elegans. Proc Natl Acad Sci U S A 112: 11690-11695

Cho Y, Porto DA., Hwang H, Grundy LJ, Schafer WR, Lu H (2017) Automated and controlled mechanical stimulation and functional imaging: In vivo in C. elegans. Lab on a chip, 17, 15, 2609 – 2618

Cho Y, N. Oakland DN, Lee SA, Schafer WR and Lu H (2018) On-chip functional neuroimaging with mechanical stimulation in Caenorhabditis elegans larvae for studying development and neural circuits. Lab on a chip 18, 601–609

Collet J, Spike CA, Lundquist EA, Shaw JE, Herman RK (1998) Analysis of osm-6, a gene that affects sensory cilium structure and sensory neuron function in Caenorhabditis elegans. Genetics 148: 187-200

DeVault L, Li T, Izabel S, Thompson-Peer KL, Jan LY, Jan YN (2018) Dendrite regeneration of adult Drosophila sensory neurons diminishes with aging and is inhibited by epidermal-derived matrix metalloproteinase. Genes Dev 32: 402-414

Dong X, Liu OW, Howell AS, Shen K (2013) An extracellular adhesion molecule complex patterns dendritic branching and morphogenesis. Cell 155: 296-307

Dong X, Shen K, Bülow HE (2015) Intrinsic and extrinsic mechanisms of dendritic morphogenesis. Annu Rev Physiol 77: 271-300

Driscoll M, Chalfie M (1991) The *mec*-4 gene is a member of a family of *Caenorhabditis elegans* genes that can mutate to induce neuronal degeneration. Nature 349: 588-593

Eastwood A L., Sanzeni A, Petzold B C, Park S J, Vergassola M, Pruitt B L, and Goodman M B. (2015) Tissue mechanics govern the rapidly adapting and symmetrical response to touch. PNAS, E6955–E6963

Fehlauer H, Nekimken AL, Kim Anna A, Pruitt BL, Goodman MB, Krieg M (2018) Using a Microfluidics Device for Mechanical Stimulation and High Resolution Imaging of *C. elegans.* J Vis Exp. (132):56530

Fox K, Wong RO (2005) A comparison of experience-dependent plasticity in the visual and somatosensory systems. Neuron 48: 465-477

Gat A, Pechuk V, Peedikayil-Kurien S, Karimi S, Goldman G, Sela S, Lubliner J, Krieg M, and Oren-Suissa M (2023) Integration of spatially opposing cues by a single interneuron guides decision-making in C. elegans. Cell reports 42, 113075

Ghiretti AE, Moore AR, Brenner RG, Chen LF, West AE, Lau NC, Van Hooser SD, Paradis S (2014) Rem2 Is an Activity-Dependent Negative Regulator of Dendritic Complexity In Vivo. J Neurosci 34: 392-407

Gillespie PGW, R. G. (2001) Molecular basis of mechanosensory transduction. Nature 413: 194-202

Gobetto MN, Gonzalez-Inchauspe C, Uchitel OD (2021) Histamine and Corticosterone Modulate Acid Sensing Ion Channels (ASICs) Dependent Long-term Potentiation at the Mouse Anterior Cingulate Cortex. Neurosci Behav Physiol 460: 145-160

Goodman CS, Shatz CJ (1993) Developmental mechanisms that generate precise patterns of neuronal connectivity. Cell 72 Suppl: 77-98

Goodman MB, Sengupta P (2019) How Caenorhabditis elegans Senses Mechanical Stress, Temperature, and Other Physical Stimuli. Genetics 212: 25-51

Gyorffy BA, Kun J, Torok G, Bulyaki E, Borhegyi Z, Gulyassy P, Kis V, Szocsics P, Micsonai A, Matko J, Drahos L, Juhasz G, Kekesi KA, Kardos J (2018) Local apoptotic-like mechanisms underlie complement-mediated synaptic pruning. Proc Natl Acad Sci U S A 115: 6303-6308

Hall DH, Treinin M (2011) How does morphology relate to function in sensory arbors? Trends Neurosci 34: 443-51

Halpain S (2018) Avoiding Sibling Conflict: Lessons from Dendrite Self-Avoidance in C. elegans. Neuron 98: 864

Harlow HF, Dodsworth RO, Harlow MK (1965) Total social isolation in monkeys. Proc Natl Acad Sci U S A 54: 90-97

Hausser M, Mel B (2003) Dendrites: bug or feature? Curr Opin Neurobiol 13: 272-283

Hedgecock EM, Sulston JE, Thomson JN (1983) Mutations affecting programmed cell deaths in the nematode *Caenorhabditis elegans*. Science 220: 1277-1279

Heiman MG, Bülow HE (2024) Dendrite morphogenesis in Caenorhabditis elegans. Genetics 227(2), iyae056

Hill AS, Ben-Shahar Y (2018) The synaptic action of Degenerin/Epithelial sodium channels. Channels 12: 262-275

Holtmaat A, Svoboda K (2009) Experience-dependent structural synaptic plasticity in the mammalian brain. Nat Rev Neurosci 10: 647-658

Hu HT, Huang TN, Hsueh YP (2020) KLHL17/Actinfilin, a brain-specific gene associated with infantile spasms and autism, regulates dendritic spine enlargement. J Biomed Sci 27: 103

Huang M, Chalfie M (1994) Gene interactions affecting mechanosensory transduction in Caenorhabditis elegans. Nature 367: 467-470

Huebschman JL, Corona KS, Guo Y, Smith LN (2020) The Fragile X Mental Retardation Protein Regulates Striatal Medium Spiny Neuron Synapse Density and Dendritic Spine Morphology. Front Mol Neurosci 13: 161

Husson SJ, Costa WS, Wabnig S, Stirman JN, Watson JD, Spencer WC, Akerboom J, Looger LL, Treinin M, Miller DM, 3rd, Lu H, Gottschalk A (2012) Optogenetic analysis of a nociceptor neuron and network reveals ion channels acting downstream of primary sensors. Curr Biol 22: 743-752

Inberg S, Meledin A, Kravtsov V, Iosilevskii Y, Oren-Suissa M, Podbilewicz B (2019) Lessons from worm dendritic patterning. Annual review of neuroscience 42: 365-383

Inberg S, Podbilewicz B (2018) Sensory experience controls dendritic structure and behavior by distinct pathways involving degenerins. bioRxiv [Preprint]. doi: 10.1101/436758)

Inberg S, Iosilevskii Y, Podbilewicz B (2021) Sensory experience controls dendritic structure and behavior by distinct pathways involving degenerins. bioRxiv [Preprint]. doi: 10.1101/436758)

Iosilevskii Y, Podbilewicz B (2021) Programmed cell fusion in development and homeostasis. Curr Top Dev Biol 144: 215-244

Iosilevskii Y, Podbilewicz B (2024) The PVD neuron has male-specific structure and mating function in *C. elegans.* bioRxiv 2024.05.19.594847

Jan YN, Jan LY (2010) Branching out: mechanisms of dendritic arborization. Nat Rev Neurosci 11: 316-328

Karimi S, Gat A, Agazzi C, Oren-Suissa M, and Krieg M (2024) Automated dual olfactory device for studying head/tail chemosensation in Caenorhabditis elegans. APL Bioeng. 8(2), 026104. https://doi.org/10.1063/5.0187441

Katta S, Krieg M, Goodman MB. (2015) Feeling force: physical and physiological principles enabling sensory mechanotransduction. Annu Rev Cell Dev Biol. 31:347-371.

Katz EM, Chu DK, Casey KM, Jampachaisri K, Felt SA, Pacharinsak C (2020) The Stability and Efficacy of Tricaine Methanesulfonate (MS222) Solution After Long-Term Storage. J Am Assoc Lab Anim Sci. 12: 393-400

Katz LC, Shatz CJ (1996) Synaptic activity and the construction of cortical circuits. Science 274: 1133-1138

Kellenberger S, Schild L (2002) Epithelial Sodium Channel/Degenerin Family of Ion Channels: A Variety of Functions for a Shared Structure. Physiol Rev 82: 735-767

Kim E, Sun L, Gabel CV, Fang-Yen C (2013) Long-Term Imaging of Caenorhabditis elegans Using Nanoparticle-Mediated Immobilization. PLoS One 8: e53419

Kolb B, Whishaw IQ (1998) Brain plasticity and behavior. Annu Rev Psychol 49: 43-64

Kravtsov V, Oren-Suissa M, Podbilewicz B (2017) The fusogen AFF-1 can rejuvenate the regenerative potential of adult dendritic trees via self-fusion. Development 144: 2364-2374

Krieg M, Pidde A, Das R (2022) Mechanosensitive body–brain interactions in *Caenorhabditis elegans.* Current Opinion in Neurobiology 75:102574

Kuhlman SJ, O'Connor DH, Fox K, Svoboda K (2014) Structural Plasticity within the Barrel Cortex during Initial Phases of Whisker-Dependent Learning. J Neurosci 34: 6078-6083

Li W, Kang L, Piggott BJ, Feng Z, Xu XZ (2011) The neural circuits and sensory channels mediating harsh touch sensation in Caenorhabditis elegans. Nat Commun 2: 315

Luo L (2002) Actin Cytoskeleton Regulation in Neuronal Morphogenesis and Structural Plasticity. Annu Rev Cell Dev Biol 18: 601-635

Mango D, Nistico R (2020) Role of ASIC1a in Normal and Pathological Synaptic Plasticity. Reviews of physiology, biochemistry and pharmacology 177: 83-100

Maures TJ, Booth LN, Benayoun BA, Izrayelit Y, Schroeder FC, Brunet A (2014) Males shorten the life span of C. elegans hermaphrodites via secreted compounds. Science 343: 541-4

Miller-Fleming TW, Petersen SC, Manning L, Matthewman C, Gornet M, Beers A, Hori S, Mitani S, Bianchi L, Richmond J, Miller DM (2016) The DEG/ENaC cation channel protein UNC-8 drives activity-dependent synapse removal in remodeling GABAergic neurons. eLife 5

Nagerl UV, Eberhorn N, Cambridge SB, Bonhoeffer T (2004) Bidirectional Activity-Dependent Morphological Plasticity in Hippocampal Neurons. Neuron 44: 759-767

Nekimken A, Holger F, Kim A, Manosalvas-KS, Ladpl P, Memon F, Gopisetty D, Sanchez V, Goodman MB, Pruitt BL, and Krieg M (2017) Pneumatic stimulation of C. elegans mechanoreceptor neurons in a microfluidic trap, Lab Chip 17(6): 1116–1127

Oren-Suissa M, Gattegno T, Kravtsov V, Podbilewicz B (2017) Extrinsic Repair of Injured Dendrites as a Paradigm for Regeneration by Fusion in Caenorhabditis elegans. Genetics 206: 215-230

Oren-Suissa M, Hall D, Treinin M, Shemer G, Podbilewicz B (2010) The Fusogen EFF-1 Controls Sculpting of Mechanosensory Dendrites. Science 328: 1285-1288

Porta-de-la-Riva M, Gonzalez AC, Sanfeliu-Cerdán N, Karimi S, Malaiwong, Pidde A, Curiel LFM, Fernandez P, González-Bolívar S, Hurth C, Krieg M (2023) Neural engineering with photons as synaptic transmitters. Nature methods 20, 761–76

Rose JK, Sangha S, Rai S, Norman KR, Rankin CH (2005) Decreased sensory stimulation reduces behavioral responding, retards development, and alters neuronal connectivity in Caenorhabditis elegans. J Neurosci 25: 7159-68

Roy Choudhury A, Groflhans J, Kong D (2021) Ion Channels in Epithelial Dynamics and Morphogenesis. Cells 10: 2280

Salzberg Y, Diaz-Balzac CA, Ramirez-Suarez NJ, Attreed M, Tecle E, Desbois M, Kaprielian Z, Bülow HE (2013) Skin-Derived Cues Control Arborization of Sensory Dendrites in Caenorhabditis elegans. Cell 155: 308-20

Salzberg Y, Ramirez-Suarez NJ, Bülow HE (2014) The proprotein convertase KPC-1/furin controls branching and self-avoidance of sensory dendrites in Caenorhabditis elegans. PLoS genetics 10: e1004657

Sanfeliu-Cerdán N, Català-Castro F, Mateos B, Garcia-Cabau C, Ribera M, Ruider I, Porta-de-la-Riva Montserrat Canals-Calderón A, Wieser S, Salvatella X, Krieg M (2023). A MEC-2/stomatin condensate liquid-to-solid phase transition controls neuronal mechanotransduction during touch sensing. Nature cell biology, 25(11), 1590–1599

Sawin ER, Ranganathan R, Horvitz HR (2000) C. elegans locomotory rate is modulated by the environment through a dopaminergic pathway and by experience through a serotonergic pathway. Neuron 26: 619-631

Setty H, Salzberg Y, Karimi S, Berent-Barzel E, Krieg M, Oren-Suissa M (2022) Sexually dimorphic architecture and function of a mechanosensory circuit in C. elegans. Nature communications 13:6825

Shi S, Luke CJ, Miedel MT, Silverman GA, Kleyman TR (2016) Activation of the Caenorhabditis elegans Degenerin Channel by Shear Stress Requires the MEC-10 Subunit. J Biol Chem 291: 14012-14022

Shi S, Mutchler SM, Blobner BM, Kashlan OB, Kleyman TR (2018) Pore-lining residues of MEC-4 and MEC-10 channel subunits tune the Caenorhabditis elegans degenerin channel's response to shear stress. J Biol Chem 293: 10757-10766

Sin WC, Haas K, Ruthazer ES, Cline HT (2002) Dendrite growth increased by visual activity requires NMDA receptor and Rho GTPases. Nature 419: 475-480

Smith CJ, Watson JD, Spencer WC, O'Brien T, Cha B, Albeg A, Treinin M, Miller DM, 3rd (2010) Time-lapse imaging and cell-specific expression profiling reveal dynamic branching and molecular determinants of a multi-dendritic nociceptor in C. elegans. Dev Biol 345: 18-33

Star EN, Kwiatkowski DJ, Murthy VN (2002) Rapid turnover of actin in dendritic spines and its regulation by activity. Nat Neurosci 5: 239-246

Stein IS, Park DK, Claiborne N, Zito K (2021) Non-ionotropic NMDA receptor signaling gates bidirectional structural plasticity of dendritic spines. Cell reports 34: 108664

Sulston JE, Schierenberg E, White JG, Thomson JN (1983) The Embryonic Cell Lineage of the Nematode *Caenorhabditis elegans*. Dev Biol 100: 64-119

Suzuki H, Kerr R, Bianchi L, Frokjaer-Jensen C, Slone D, Xue J, Gerstbrein B, Driscoll M, Schafer WR (2003) In vivo imaging of C. elegans mechanosensory neurons demonstrates a specific role for the MEC-4 channel in the process of gentle touch sensation. Neuron 39: 1015-1017

Tao L, Porto D, Li Z, Fechner S, Lee SA, Goodman MB, Xu XZS, Lu H, Shen K (2019) Parallel Processing of Two Mechanosensory Modalities by a Single Neuron in C. elegans. Dev Cell 51: 617-631 e3

Tavosanis G (2012) Dendritic structural plasticity. Dev Neurobiol 72: 73-86

Tendilla-Beltran H, Antonio Vazquez-Roque R, Judith Vazquez-Hernandez A, Garces-Ramirez L, Flores G (2019) Exploring the Dendritic Spine Pathology in a Schizophrenia-related Neurodevelopmental Animal Model. Neuroscience 396: 36-45

Tsalik EL, Niacaris T, Wenick AS, Pau K, Avery L, Hobert O (2003) LIM homeobox gene-dependent expression of biogenic amine receptors in restricted regions of the C. elegans nervous system. Dev Biol 263: 81-102

Vaillant AR, Zanassi P, Walsh GS, Aumont A, Alonso A, Miller FD (2002) Signaling mechanisms underlying reversible, activity-dependent dendrite formation. Neuron 34: 985-998

Way JC, Chalfie M (1988) mec-3, a homeobox-containing gene that specifies differentiation of the touch receptor neurons in C. elegans. Cell 54: 5-16

Welsh MJ, Price MP, Xie J (2002) Biochemical Basis of Touch Perception: Mechanosensory Function of Degenerin/Epithelial Na+ Channels. J Biol Chem 277: 2369-2372

Wiesner T, Bilodeau A, Bernatchez R, Deschenes A, Raulier B, De Koninck P, Lavoie-Cardinal F (2020) Activity-Dependent Remodeling of Synaptic Protein Organization Revealed by High Throughput Analysis of STED Nanoscopy Images. Front Neural Circuits 14: 57

Wilbrecht L, Holtmaat A, Wright N, Fox K, Svoboda K (2010) Structural Plasticity Underlies Experience-Dependent Functional Plasticity of Cortical Circuits. J Neurosci 30: 4927-4932

Wong RO, Ghosh A (2002) Activity-dependent regulation of dendritic growth and patterning. Nat Rev Neurosci 3: 803-812

Xu T, Yu X, Perlik AJ, Tobin WF, Zweig JA, Tennant K, Jones T, Zuo Y (2009) Rapid formation and selective stabilization of synapses for enduring motor memories. Nature 462: 915-919

Yang G, Pan F, Gan WB (2009) Stably maintained dendritic spines are associated with lifelong memories. Nature 462: 920-924

Younger MA, Muller M, Tong A, Pym EC, Davis GW (2013) A Presynaptic ENaC Channel Drives Homeostatic Plasticity. Neuron 79: 1183-1196

Yu X, Zuo Y (2011) Spine plasticity in the motor cortex. Curr Opin Neurobiol 21: 169-174

Zhang Y, Cudmore RH, Lin DT, Linden DJ, Huganir RL (2015) Visualization of NMDA receptor–dependent AMPA receptor synaptic plasticity in vivo. Nat Neurosci 18: 402-407

Zhou Z, Hong EJ, Cohen S, Zhao WN, Ho HY, Schmidt L, Chen WG, Lin Y, Savner E, Griffith EC, Hu L, Steen JA, Weitz CJ, Greenberg ME (2006) Brain-Specific Phosphorylation of MeCP2 Regulates Activity-Dependent Bdnf Transcription, Dendritic Growth, and Spine Maturation. Neuron 52: 255-269

Zuo Y, Yang G, Kwon E, Gan WB (2005) Long-term sensory deprivation prevents dendritic spine loss in primary somatosensory cortex. Nature 436: 261-265

Figure legends

Figure 1. Mechanosensory deprivation during development reduces the behavioral response of the PVD neuron. (A) The PVD neuron dendritic tree, cell body (CB) and axon. The red arrow corresponds to the contact point with a platinum wire during posterior harsh touch, while the black arrow represents the behavioral escape response of the worm. The red dashed square represents the analyzed region around the CB. One representative candelabrum is colored by branch orders: blue primary (1°), purple secondary (2°), cyan tertiary (3°) and green quaternaries (4°). A- anterior; P- posterior; V- ventral; D-dorsal. **(B)** Schematic of the isolation protocol followed at 72 h by posterior harsh touch assay or PVD imaging of adult worms. **(C)** Isolation of embryos reduced the percentage of worms responding to harsh touch at adulthood. Crowded- black bars, Isolated- red bars. Wildtype (WT) N2 worms (Crowded, n=32; Isolated, n=32), *mec-4* (Crowded, n=52; Isolated, n=46), *mec-3* (Crowded, n=12; Isolated, n=12). *mec-4* animals were assayed as adults after 96 h to account for their slower rate of growth. **(D)** Growth in plates with chemical cues from adult hermaphrodites did not alter the reduced response rate of isolated *mec-4* animals to harsh touch (Crowded, n=33; Isolated, n=28). **(E)** Harsh touch response in crowded and isolated conditions for mutants of different DEG-ENaCs and the TRP channel *gtl-1*. WT worms (same set of worms as in Figure 1C. Crowded, n=32; Isolated, n=32), *asic-1* (Crowded, n=46; Isolated, n=30), *mec-10* (Crowded, n=38; Isolated, n=31), *degt-1* (Crowded, n=37; Isolated, n=31), *unc-8* (Crowded, n=18; Isolated, n=15), *del-1* (Crowded, n=31; Isolated, n=27), *gtl-1* (Crowded, n=27; Isolated, n=25). **(F)** MEC-10 expression in the PVD rescues *mec-10* mutants' crowded-specific reduction in response to harsh touch. All strains contain the *ser-2Prom3::Kaede* PVD marker construct, and were tested in the crowded conditions. (WT, n=42; *mec-4,* n=17; *him-5,* n=34 (*him-5* was used as WT background for several strains after cross); *him-5; mec-10,* n=35; *him-5; mec-10*; *ser2Prom3*::*mec-10*, n=33). **(G)** Isolation for 24 h in adulthood did not affect the response to harsh touch. Worms grown under crowded conditions were isolated for 24 h as young adults and compared against their crowded age-matched counterparts in their response to harsh touch (Crowded, n=25; Isolated for 24 h, n=26). The proportion of responding worms (percentage) ± standard error of proportion is shown. Fisher's exact test, *p<0.05, **p<0.01, ***p<0.001, n.s. not significant.

Figure 2. Mechanosensory deprivation and cell autonomous activity of *mec-10* affects the architecture of the PVD. (A) Schematic representation of the PVD dendritic structure, marking the morphological characteristics of interest: ectopic branches and quaternary branching geometry. Dashed lines represent ectopic branching at each order. Colors correspond to Figure 1A. (**B-G**) Both isolation and *mec-10* affect the structure of the PVD: **(B)** Isolation increases the fraction of ectopic branching, *mec-10* mutation increases ectopic branching in the crowded state. **(C)** Isolation decreases the percentage of straight quaternary branches, *mec-10* mutation decreases the percentage of straight quaternary branches in the crowded state. Crowded- black dots, isolated- red dots; WT (Crowded, n=28; Isolated n=26), *him-5* (Crowded, n=27; Isolated, n=25; *him-5* was used as WT background for several strains after cross), *him-5; mec-10* (Crowded, n=30; Isolated, n=24). **(D)** Expression of *mec-10* in the PVD on the background of *him-5; mec-10* in the crowded state reduces ectopic branching and **(E)** increases the percentage of straight quaternary branches (Crowded *him-5*, n=28; Crowded *him-5:mec-10*, n=36; Crowded *him-5:mec-10*;PVD::MEC-10, n=27). **(F-I)** Representative PVD images of WT,

mec-10 and *mec-10*; PVD::*mec-10* in different growth conditions. (Scale bar, 50 µm). **(J)** Embryo isolation with glass beads did not affect ectopic branching. **(K)** Embryo isolation with glass beads increased the percentage of straight quaternary branches (Crowded, n=28; Isolated n=26; Isolated with beads, n=22. Crowded and isolated WT are the same set of worms as in Figure 2B,C). Each dot represents a single worm. The mean ± s.e.m. are shown in blue. Box plot with median and hinges for the first and third quartile. The whiskers represent an estimated calculation of the 95% confidence interval. Kruskal-Wallis test, # # p<0.01, # # # p<0.001, Mann Whitney test with Bonferroni Correction α=0.0167. *p<0.05, ** p<0.01, *** p<0.001, n.s. not significant.

Figure 3. Adult isolation for less than 4 h affects the structure of the PVD.
(A) Isolation of crowded worms induces a time-dependent increase in the proportion of ectopic branches, and **(B)** a decrease in the number of straight quaternary branches (2 h: Crowded, n=24, Isolated, n=22; 5 h: Crowded, n=24, Isolated, n=27; 15 h: Crowded, n=3, Isolated, n=3; 24 h: Crowded, n=20, Isolated, n=21; animals imaged using polystyrene beads for immobilization, see Materials and Methods). **(C)** Isolation for 4 h induces more growth of new branches than retraction of existing ones. Ectopic branch dynamics were compared for crowded animals against their state after 4 h isolation. Imaging used 1% tricaine, see Materials and Methods. **(D)** Isolation of crowded worms for 4 h increases the ratio between ectopic/non-ectopic branches in individual animals and **(E)** reduces the percentage of straight quaternary branches (n=6). **(F)** Crowded, but not isolated worms, show dynamic reduction in the percentage of straight quaternary branches during a 3 h time lapse movie in 1% tricaine; see Videos 1 and 2 (Crowded, n=5, Isolated, n=6). **(G)** Representative time lapse frames of a crowded worm in 1% tricaine. Thick and thin arrows represent straight and non-straight quaternary branches, respectively. For **(D, E)** the lines connecting two points refer to the same crowded specimen at time 0 and after 4 h isolation. Box plot representation as in Figure 2. For **(A-B)** Mann-Whitney test, * p<0.05, *** p<0.001. For **(C-E)** Wilcoxon test (for two related samples), * p<0.05. The mean ± s.e.m. are shown for panels A-C, and F.

Figure 4. Response to harsh touch and PVD morphology are independent.
(A) Discriminant analysis shows independence of harsh touch response from the PVD's morphological classification. Squares indicate the centroids for morphological characteristics analyzed in Figure 4–figure supplement 2A-C. The response to harsh touch (Figure 4–figure supplement 1) is illustrated by its magnitude (low, <45% in yellow star; high, >65% in light blue circles). The different genotypes are numbered in the list on the right. Crowded- black, Isolated-red. **(B-E)** Isolated animals show similar PVD morphology regardless of their touch response: **(B)** isolated responding and non-responding animals are not different with regard to the fraction of ectopic branching, and **(C)** the geometry of quaternary branches (Isolated non-responding, n=18; Isolated responding, n=20). Box plot representation as in Figure 2. Mann-Whitney test. n.s. not significant. **(D, E)** Representative PVD images of responding and non-responding worms. (Scale bar, 50 µm).

Figure 5. Mechanosensory-dependent localization of degenerins and optogenetics. (A) PVD::MEC-10::mCherry localization (shown and labeled in purple, also in Figure 7) is reduced in the quaternary branches and the axon following isolation, in a *degt-1*-dependent manner (WT: Crowded, n=31; Isolated, n=27; *degt-1* mutants:

Crowded, n=23; Isolated, n=22). **(B-D)** Representative images and reconstructions for PVD::*mec-10*::mCherry localization for crowded and isolated WT worms, and crowded *degt-1* worms. (Scale bar, 50 µm). **(E)** PVD::*degt-1::*mCherry localization level is reduced at the cell body, but not in the quaternary branches or the axon, following isolation, in a *mec*-10-dependent-manner (WT: Crowded, n=33; Isolated, n=21; *mec-10* mutants: Crowded, n=28; Isolated, n=22). The percentage of expressing worms ± standard error of proportion is shown. **(F-H)** Representative images and reconstructions for PVD::*degt-1*::mCherry localization for crowded and isolated WT worms and crowded *mec-10* worms. **(I)** Isolation leads to a reduced escape response following optogenetic photoactivation of Channelrhodopsin 2 in the PVD (Crowded, n=30; Isolated, n=24, grown on All Trans Retinal. No response was observed for worms grown without All Trans Retinal). Fisher exact test, *p<0.05, **p<0.01, ***p<0.01 n.s. not significant.

Figure 6. The calcium response to mechanical stimulation shows no significant difference between crowded and isolated worms.
Mechanically induced calcium recordings of PVD of animals grown as **(A)** isolated individuals or **(B)** in crowded conditions. **i)** Stimulus profile displaying a single step, sawtooth indentation or 10 Hz `buzz'. Bottom panels show examples of negative images from experiments at pre- and post-stimulation; note PVDs' cell bodies about 200 µm to the right of the location of the mechanical stimuli. Scale bar, 100 µm. **(ii)** Kymograph of individual response for N=17 animals and N=27 animals for the crowded conditions. Green bars, time of application of a mechanical stimulus. **(iii)** Average GCaMP6s signal derived from the cell body of PVD for the duration of the recordings, black line. N = number of recordings. Mean +/- standard deviation, grey region. Inset in panel iii shows the running p-value, comparing the crowded and isolated conditions (Dashed line indicates alpha level of significance a=0.05).

Figure 7. Model of experience-induced structural and behavioral plasticity. During adulthood, mechanosensory signals maintain the structure of the PVD in crowded animals, with straight quaternary branches and fewer ectopic branches. Sensory deprivation (in isolated animals) results in ectopic dendrites, wavy branches and defects in candelabra self-avoidance. During development, mechanosensory experience alters the response to harsh touch and the crawling gait of the worm (Inberg et al., 2021), possibly through changes in MEC-10 localization in the axon and mediated by other DEG/ENaCs. Mechanosensory stimuli are a driving force for changes in the compartment specific localization of MEC-10 and DEGT-1 in the PVD, which may affect the structure of the PVD. MEC-10 is represented in blue, DEGT-1 is represented in green.

Supplementary figure legends

Figure 1–figure supplement 1. The reduction in response to harsh touch following isolation is PVD-dependent and chemosensory-independent.
(A) Isolation of gentle-touch-insensitive *mec-4* worms with glass beads partially rescues the isolation-induced reduction in harsh touch response. Experiment performed after 96 h to account for slower growth rate. Crowded, n=39; Isolated, n=42; Isolated with beads, n=31). **(B)** Isolation of *osm-6* mutants, defective in ciliated chemosensory neurons and the PDE nociceptor, resulted in reduced response to harsh touch, when compared to worms from a crowded plate. (Crowded, n=34; Isolated, n=27). **(C)** Continuous exposure to amiloride does not affect the WT response to harsh touch in the crowded conditions (Crowded with DMSO, n=54; Crowded with 3 mM amiloride, n=52). The proportion of responding worms (percentage) ± the standard error of proportion is shown. Fisher exact test, * $p<0.05$, ** $p<0.01$, n.s. not significant.

Figure 2–figure supplement 1. **The effect of isolation on the structure of the PVD is independent from the identity of the promoter driving expression of the reporter in the PVD.**
Worms expressing the PVD fluorescent marker, *dzIs53* [*pF49H12.4*::mCherry] were isolated as in Figure 1B. **(A)** Embryo isolation for 72 h increased total ectopic branching, and **(B)** reduced the percentage of straight quaternary branches (Crowded, n=20; Isolated, n=20). **(C, D)** Representative PVD images of *dzIs53* [*pF49H12.4*::mCherry] crowded and isolated adults. (Scale bar, 50 µm). Box plot description as in Figure 2. Mann Whitney test, *** $p<0.001$. One representative candelabrum is colored as in Figure 1A.

Figure 2–figure supplement 2. The PVD undergoes isolation-dependent structural plasticity in the presence of pheromonal signals in the plate.
Both crowded and isolated worms were pre-exposed to pheromonal signals, released by *glp-4* worms (~40 worms for 96 h. The *glp-4* worms were taken out of the plate and the isolation protocol described in Figure 1B was used). **(A)** Chemical stimulation of plates with *glp-4*, followed by egg isolation, increased the fraction of ectopic branching, and **(B)** decreased straight quaternary branches (Crowded, n=24; Isolated, n=20). **(C, D)** Representative PVD images for crowded and isolated worms with chemical stimulation of the plates. White arrow, ectopic branching. (Scale bar, 50 µm). Box plot representation as in Fig 2. Mann Whitney test, *** $p<0.001$. One representative candelabrum is colored as in Figure 1A.

Figure 2–figure supplement 3. The effect of isolation on the structure of PVD is not mediated by the gentle touch mechano-sensory neurons.
(A) Description of the protocol for the isolation of *mec-4* eggs for 96 h (the experiment was performed for 96 h since the worms were L4s or very young adults at 72 h), followed by PVD imaging. **(B)** Isolation of the gentle touch impaired strain, *ser-2Prom3*::Kaede; *mec-4*, increased total ectopic branching, and **(C)** reduced the percentage of straight quaternary branching (Crowded, n=20; Isolated, n=21). **(D, E)** Representative PVD images derived from crowded worms and isolated eggs. White arrow, ectopic branching (Scale bar, 50 µm). Box plot representation as in Figure 2. Mann Whitney test with Bonferroni correction ** $p<0.01$. One representative candelabrum is colored as in Figure 1A.

Figure 2–figure supplement 4. Isolation of eggs for 48 h and adults for 24 h is sufficient to induce changes in the structure of the PVD.
(A) Schematic protocol for the isolation of WT eggs for 48 h and adults for 24 h, followed by PVD imaging. **(B)** Isolation of eggs for 48 h (resulted in young adult worms) did not affect the number of ectopic branches, and **(C)** decreased the percentage of straight quaternary branching (Crowded, n=30; Isolated, n=24). **(D, E)** Representative PVD images for crowded worms and isolated eggs. (Scale bar, 50 µm). **(F)** Isolation of young adult worms for 24 h increased the fraction of ectopic branching, and **(G)** reduced the percentage of straight quaternary branches (Crowded, n=20; Isolated adults for 24 h, n=21). **(H, I)** Representative pictures from the PVD images for crowded and matched animal isolated as young adult for 24 h. A small arrow marks a self-avoidance defect. Box plot representation as in Figure 2. Mann Whitney test, ** $p<0.01$, *** $p<0.001$, n.s. not significant. One representative candelabrum is colored as in Figure 1A.

Figure 3–figure supplement 1. Four hours are sufficient to induce an increase in ectopic branching and a decrease in percentage of straight branches.
Left image is from a young adult grown in crowded conditions. Following confocal imaging this worm was isolated for 4 h and imaged again (right image). Straight terminal branches (black arrows, left image) became non-straight and there are new ectopic branches (white arrows, right image; see quantitative analyses in Figure 3D,E).

Figure 3–figure supplement 2. Activity-modulating pharmacological agents affect the structure and the dynamics of PVD branch growth and retraction.
(A-D) Blocking DEG/ENaC with 3 mM amiloride in crowded plate conditions affects the structure of the PVD. **(A)** Increased the fraction of ectopic branches, and **(B)** decreased the percentage of straight quaternary branches, (Crowded with DMSO, n=23; Crowded with amiloride n=27). **(C, D)** Representative PVD images in DMSO- and amiloride-treated worms. One representative candelabrum is colored as in Figure 1A (Scale bar, 25 µm). **(E-G)** A mixture containing 0.01% tetramisole and 0.1% tricaine induced more dendritic growth than retraction in crowded conditions **(E;** Crowded: n=5; Isolated, n=5). Representative images from time lapse movies demonstrating dynamic outgrowth of branching under tricaine-tetramisole anesthetic mixture for crowded **(F)** and isolated worms **(G)**. **(H-J)** 1% tricaine induced more dendritic retraction than growth. In addition, more dendritic growth was measured for isolated worms, compared to crowded (**H**; Crowded: n=6; Isolated, n=6). Representative time lapse movies demonstrating dynamic retraction of branching for crowded **(I)** and isolated **(J)** worms**;** see Videos 1 and 2. Blue arrowheads, branch growth; red arrowheads, branch retraction; bar for panel 'I', 25 µm. Box plots are as represented in Figure 2. Mann Whitney test *$p<0.05$, ** $p<0.01$. For **(E,H)** t-Test. *$p<0.05$, *** $p<0.001$, n.s. not significant.

Figure 4–figure supplement 1. The DEG/ENaC *asic-1* and *mec-10* mediate experience-dependent behavioral plasticity following isolation.
Posterior harsh touch assay was performed for crowded and isolated WT and DEG-ENaC mutants, similar to the procedure described in Figure 1B. Seven combinations of DEG-ENaC mutants were tested for the isolation effect on response to harsh touch. Isolated worms were compared to crowded worms from the same strain. N2 worms (The same set of worms as in Figure 1C. Crowded, n=32; Isolated, n=32), *asic-1* (Crowded, n=46; Isolated, n=30), *mec-10* (Crowded, n=38; Isolated, n=31), *degt-1* (Crowded, n=37; Isolated, n=31), *asic-1; mec-10* (Crowded, n=20; Isolated, n=22), *mec-10*; *degt-1*

(Crowded, n=40; Isolated, n=36), *asic-1*; *degt-1* (Crowded, n=35; Isolated, n=34), *asic-1*; *mec-10; degt-1* (Crowded, n=52; Isolated, n=50). The proportion (percentage) of responding worms ± the standard error of proportion is shown. Fisher exact test, *p<0.05, *** p<0.001, n.s. not significant.

Figure 4–figure supplement 2. The DEG-ENaCs, *mec-10* and *degt-1*, mediate mechanosensory dependent structural changes in the PVD.
Mutants of DEG-ENaC were isolated and were compared to crowded animals from the same strain, similar to the procedure described in Figure 1B. **(A)** Three DEG-ENaC mutants: *degt-1, mec-10; degt-1*, and *asic-1*; *mec-10; degt-1* show no difference between crowded and isolated worms in terms of ectopic branching. In addition, crowded *mec-10 and degt-1* animals increased the number of ectopic branches compared to crowded WT worms. **(B)** *mec-10; degt-1* mutants retain a high percentage of straight quaternary branches following isolation, while *mec-10* and *degt-1* single mutants have fewer straight branches compared with crowded WT animals, which decrease further upon isolation. **(C)** The increase in self-avoidance defects following isolation is DEG-ENaC dependent. WT (The same set of worms as shown in Figure 2A, B. Crowded, n=28; Isolated, n=26), *asic-1* (Crowded, n=22; Isolated, n=25), *mec-10* (Crowded, n=27; Isolated, n=21. The same set of worms as shown in Figure A, B), *degt-1* (Crowded, n=28; Isolated, n=24), *asic-1; mec-10* (Crowded, n=30; Isolated, n=31), *mec-10*; *degt-1* (Crowded, n=26; Isolated, n=28), *asic-1*; *degt-1* (Crowded, n=23; Isolated, n=22), *asic-1*; *mec-10; degt-1* (Crowded, n=23; Isolated, n=21). **(D)** Representative PVD images for crowded and isolated worms of WT and seven different DEG-ENaC mutants. (Scale bar, 50 µm). The mean ± s.e.m. are shown. Mann Whitney test, *p<0.05, ** p<0.01, *** p<0.001, n.s. not significant. One representative candelabrum is colored as in Figure 1A.

Figure 4–figure supplement 3. Isolation induces increase in loss of self-avoidance defects, in a *mec-10* dependent manner. (A) Schematic representation of the PVD dendritic structure, marking a self-avoidance defect, in which two candelabra overlap. Colors correspond to Figure 2A. **(B)** Isolation increases the percentage of self-avoidance defects between two adjacent candelabra. WT (Crowded, n=28; Isolated n=26), *him-5* (Crowded, n=27; Isolated, n=25; *him-5* was used as WT background for several strains after cross), *him-5; mec-10* (Crowded, n=30; Isolated, n=24). **(C)** Overexpression of MEC-10 in the PVD does not affect the percentage of self-avoidance defects seen in *mec-10* crowded animals. Crowded *him-5* (n=28), crowded *him-5; mec-10* (n=36), crowded *him-5; mec-10;* PVD::MEC-10 (n=27). **(D)** Isolation with glass beads reduced the percentage of self-avoidance defects, compared to isolated worms without beads (Crowded, n=28; Isolated n=26; Isolated with beads, n=22. Crowded and isolated are the same worms as used in Figure 2B-C). **(E)** Isolation during adulthood increases the percentage of self-avoidance defects in a time-dependent manner (2 h: Crowded, n=24, Isolated adults for 2 h, n=22; 5 h: Crowded, n=24, Isolated adults for 5 h, n=27; 15 h: Crowded, n=3, Isolated adults for 15 h, n=3; 24 h: Crowded, n=20, Isolated adults for 24 h, n=21)**. (F)** The percentage of self-avoidance defects is not correlated with the response to harsh touch (Isolated non-responding, n=18; Isolated responding, n=20). **(G)** Worms from a different strain and fluorescent marker, *dzIs53* [*pF49H12.4*::mCherry], were isolated as eggs for 72 h and compared to crowded worms from the same strain**.**

Isolated worms increased the percentage of self-avoidance defects between two adjacent candelabra (Crowded, n=20; Isolated, n=20). **(H)** Blocking DEG/ENaC does not affect the percentage of self-avoidance defects (Crowded DMSO, n=23; Crowded 3 mM amiloride, n=27). **(I)** Both crowded and isolated worms were pre-exposed to pheromonal signals, released by *glp-4* worms (~40 worms for 96 h). The *glp-4* worms were taken out of the plate and the isolation protocol described in Figure 1B was used. Isolation increased the percentage of self-avoidance defects (Crowded, n=24; Isolated, n=20). **(J)** Isolation of the gentle touch impaired strain, *ser-2Prom3*::Kaede; *mec-4* increased the percentage of self-avoidance defects after isolation of eggs. (Crowded, n=20; Isolated, n=21). **(K)** Isolation of eggs for 48 h did not affect the percentage of self-avoidance defects (Crowded, n=30; Isolated, n=24). **(L)** Isolation of young adult worms for 24 h increased the percentage of self-avoidance defects (Crowded, n=20; Isolated adults for 24 h, n=21). Each dot represents a single worm. Box plots are as represented in Figure 2. Kruskal-Wallis test, # $p<0.05$, # # # $p<0.001$, Mann Whitney test with Bonferroni Correction $\alpha=0.0167$. *$p<0.05$, ** $p<0.01$, *** $p<0.001$, n.s. not significant.

Figure 5–figure supplement 1. Optogenetic stimulation of isolated worms does not affect the morphology of the PVD. Worms were grown isolated with (n=8) and without (n=10) all trans retinal and subjected to 4 h light stimulation at 488 nm. Light stimulation with all trans retinal does not affect the amount of ectopic branching **(A)**, the geometry of the quaternary branches **(B)** or the the proportion of self-avoidance defects **(C)**. n.s. not significant. The mean ± s.e.m. are shown for panels A-C.

Figure 6–figure supplement 1. Basal Calcium dynamics are indistinguishable for crowded and isolated worms. The 90-second calcium dynamics of the PVD were measured in crowded (n=16) and isolated (n=17) worms. **(A)** Heatmaps representing the calcium activity for each worm. Note that the third isolated worm had a spontaneous Ca^{2+} activation. **(B)** The population averages for calcium dynamics. **(C)** The distribution of neuronal activity change across the populations of crowded and isolated worms.

Figure 6–figure supplement 2. Calcium response in the PVD is sensitive to both onset and offset of the mechanical stimulus signals. Mechanically induced calcium recordings of PVD of animals in a micromechanical device. **(A)** The GCaMP6s signal derived from the PVD before, during and after application of a mechanosensory force within a micromechanical device. The cell body of the PVD is surrounded by a dashed circle. Scale bars, 100 μm. Note, to pressure channels fingers were actuated simultaneously in this particular experiment. **(B)** Quantification of GCaMP6s signal with the corresponding time frames indicated by arrows. Green region shows time of single step stimulus. See Video 7.

Video legends

Video 1. **Time lapse of cell body and arborizations of a wildtype young adult grown under crowded conditions and anesthetized with 1% tricaine.** Red arrows point to retracting branches. See Figure 3 - figure supplement 2I for more details.

Video 2. **Time lapse of cell body and arborizations of a wildtype young adult grown in isolated conditions and anesthetized with 1% tricaine.** Red arrows point to retracting branches. See Figure 3 - figure supplement 2J for more details.

Video 3. **Localization pattern of MEC-10::mCherry in the PVD crowded adult.** MEC-10 is localized in moving vesicles, indicated by red arrow. Six z-stack series (~60 optical slices for each) were taken around the cell body every 3 minutes.

Video 4. **Localization pattern of MEC-10::mCherry in the PVD for crowded adult.** MEC-10 is localized in moving vesicles, indicated by red arrow. At time 00:00 quaternary branches can be seen. Six z-stack series (~60 optical slices for each) were taken around the cell body every 2 minutes.

Video 5. Calcium dynamics in the PVD of an isolated worm after mechanosensory stimulation. PVD cell body received ipsilateral application of a mechanical stimulus, the calcium responses from the PVD were measured. See Figure 6 for more details. Scale bar, 40 µm.

Video 6. Calcium dynamics in the PVD of a representative crowded worm after mechanosensory stimulation. PVD cell body received ipsilateral application of a mechanical stimulus, the calcium responses from the PVD were measured. See Figure 6 for more details. Scale bar, 40 µm.

Video 7. Calcium dynamics in the PVD is sensitive to both onset and offset signals. PVD cell body received ipsilateral application of a mechanical stimulus and responded by increase in calcium signal for both the onset and offset stimulations. See Figure S14 for more details. Scale bar, 40 µm.

Supplementary file legend

Supplementary file 1a. List of strains and transgenes used in this work

Supplementary file 1b. List of primers used in this work

Supplementary References

Titles for the Source Data

Figure 1-source data 1.
Original data file for Figure 1 graphs on mechanosensory deprivation during development reduces the behavioral response of the PVD neuron.

Figure 1-figure supplement 1-source data 1.
Original data file for Figure 1-figure supplement 1 on the reduction in response to harsh touch following isolation is PVD-dependent and chemosensory-independent.

Figure 2-source data 1.
Original data file for Figure 2 graphs on mechanosensory deprivation and cell autonomous activity of mec-10 affects the architecture of the PVD.

Figure 2-figure supplement 1-source data 1.
Data for Figure 2-figure supplement 1 on the effect of isolation on the structure of the PVD is independent from the promoter driving expression of the reporter in the PVD.

Figure 2-figure supplement 2-source data 1.
Original data for Figure 2-figure supplement 2 on the PVD undergoes isolation-dependent structural plasticity in the presence of pheromonal signals in the plate.

Figure 2-figure supplement 3-source data 1.
Original data for Figure 2-figure supplement 3 graphs on the effect of isolation on the structure of PVD is not mediated by the gentle touch mechano-sensory neurons.

Figure 2-figure supplement 4-source data 1.
Original data for Figure 2-figure supplement 4 graphs on isolation of eggs for 48 h and adults for 24 h is sufficient to induce changes in the structure of the PVD.

Figure 3-source data 1.
Original data file for Figure 3 graphs on adult isolation for less than 4 h affects the structure of the PVD.

Figure 3-figure supplement 2-source data 1.
Original data for Figure 3 supplement 2 graphs on activity-modulating pharmacological agents affect the structure and the dynamics of PVD branch growth and retraction.

Figure 4-source data 1.
Original data file for Figure 4 graphs on response to harsh touch and PVD morphology are independent.

Figure 4-figure supplement 1-source data 1.
Original data for Figure 4-figure supplement 1 on the DEG/ENaC *asic-1* and *mec-10* mediate experience-dependent behavioral plasticity following isolation.

Figure 4-figure supplement 2-source data 1.

Original data for Figure 4-figure supplement 2 on the DEG-ENaCs, *mec-10* and *degt-1*, mediate mechanosensory dependent structural changes in the PVD.

Figure 4-figure supplement 3-source data 1.
Original data for Figure 4-figure supplement 3 on isolation induces increase in loss of self-avoidance defects, in a *mec-10* dependent manner.

Figure 5-source data 1.
Original data file for Figure 5 graphs on mechanosensory-dependent localization of degenerins and optogenetics.

Figure 5-figure supplement 1-source data 1.
Original data file for Figure 5-figure supplement 1 on optogenetic stimulation of isolated worms does not affect the morphology of the PVD.

Figure 6-source data 1.
Original data file for Figure 6 graphs on calcium response to mechanical stimulation.

Figure 6-figure supplement 1-source data 1.
Original data file for Figure 6-figure supplement 1 on basal Calcium dynamics are indistinguishable for crowded and isolated worms.

Figure 6-figure supplement 2-source data 1.
Original data file for Figure 6-figure supplement 2 on Calcium response in the PVD is sensitive to both onset and offset of the mechanical stimulus signals.

Figure 7-figure supplement 1-source data 1.
Original data file for Figure 7-figure supplement 1 on side of plate contact alone over several hours is insufficient to elicit a difference in ectopic branching.

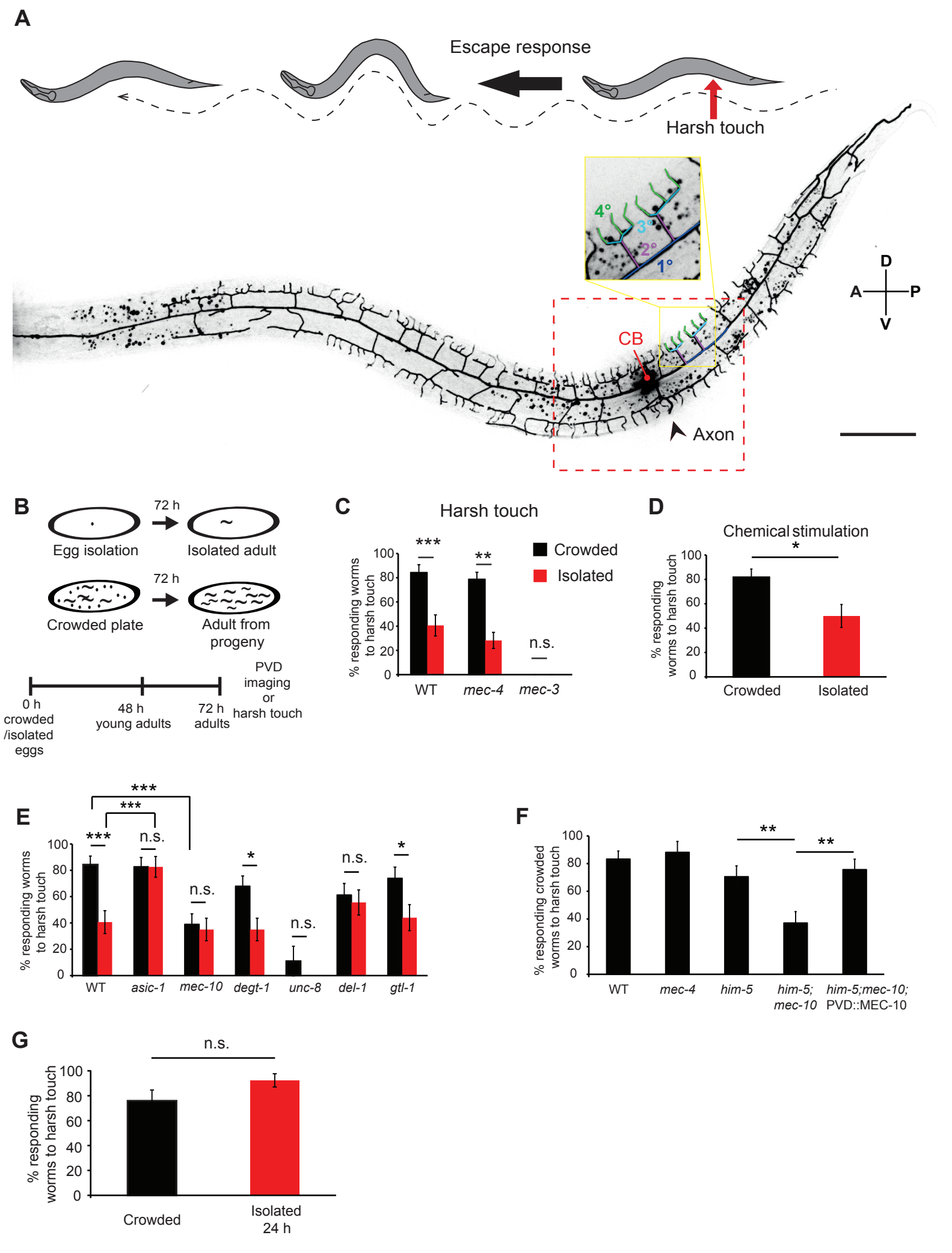
A
Escape response
Harsh touch
4°
3°
2°
1°
CB
Axon
D
A
P
V
B
72 h
Egg isolation
Isolated adult
72 h
Crowded plate
Adult from progeny
0 h crowded /isolated eggs
48 h young adults
72 h adults
PVD imaging or harsh touch
C
Harsh touch
Crowded
Isolated
% responding worms to harsh touch
***
**
n.s.
WT
mec-4
mec-3
D
Chemical stimulation
*
% responding worms to harsh touch
Crowded
Isolated
E
% responding worms to harsh touch
***
***
***
n.s.
n.s.
*
n.s.
n.s.
*
WT
asic-1
mec-10
degt-1
unc-8
del-1
gtl-1
F
% responding crowded worms to harsh touch
**
**
WT
mec-4
him-5
him-5; mec-10
him-5;mec-10; PVD::MEC-10
G
n.s.
% responding worms to harsh touch
Crowded
Isolated 24 h

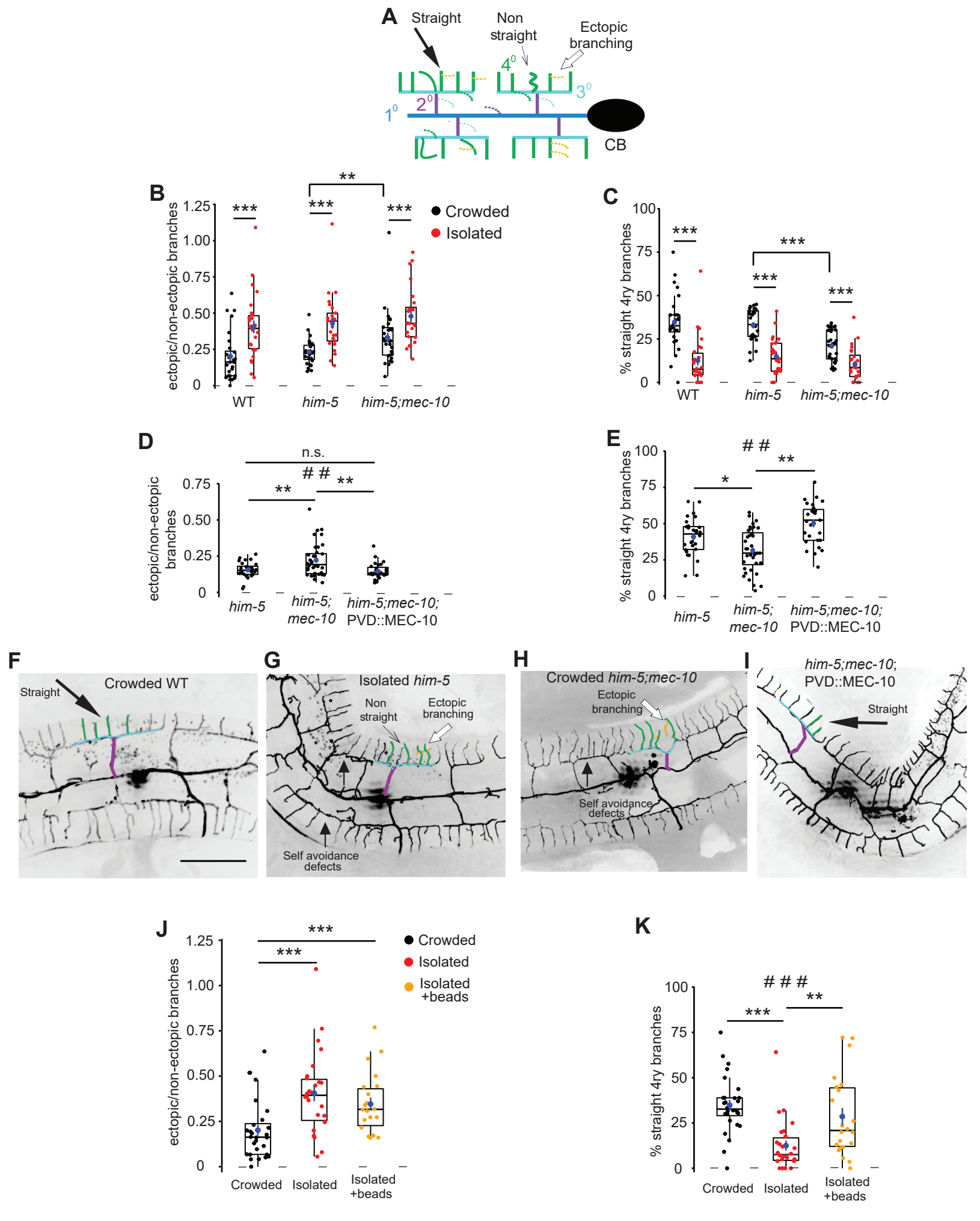
A
Straight
Non straight
Ectopic branching
4⁰
3⁰
2⁰
1⁰
CB
B
ectopic/non-ectopic branches
1.25
1.00
0.75
0.50
0.25
0
***
**
Crowded
Isolated
WT
him-5
him-5;mec-10
C
% straight 4ry branches
100
75
50
25
0
D
ectopic/non-ectopic branches
n.s.
# #
him-5
him-5; mec-10
him-5;mec-10; PVD::MEC-10
E
% straight 4ry branches
F
Crowded WT
Straight
G
Isolated him-5
Non straight
Ectopic branching
Self avoidance defects
H
Crowded him-5;mec-10
Ectopic branching
Self avoidance defects
I
him-5;mec-10; PVD::MEC-10
Straight
J
ectopic/non-ectopic branches
Crowded
Isolated
Isolated +beads
K
% straight 4ry branches
# # #

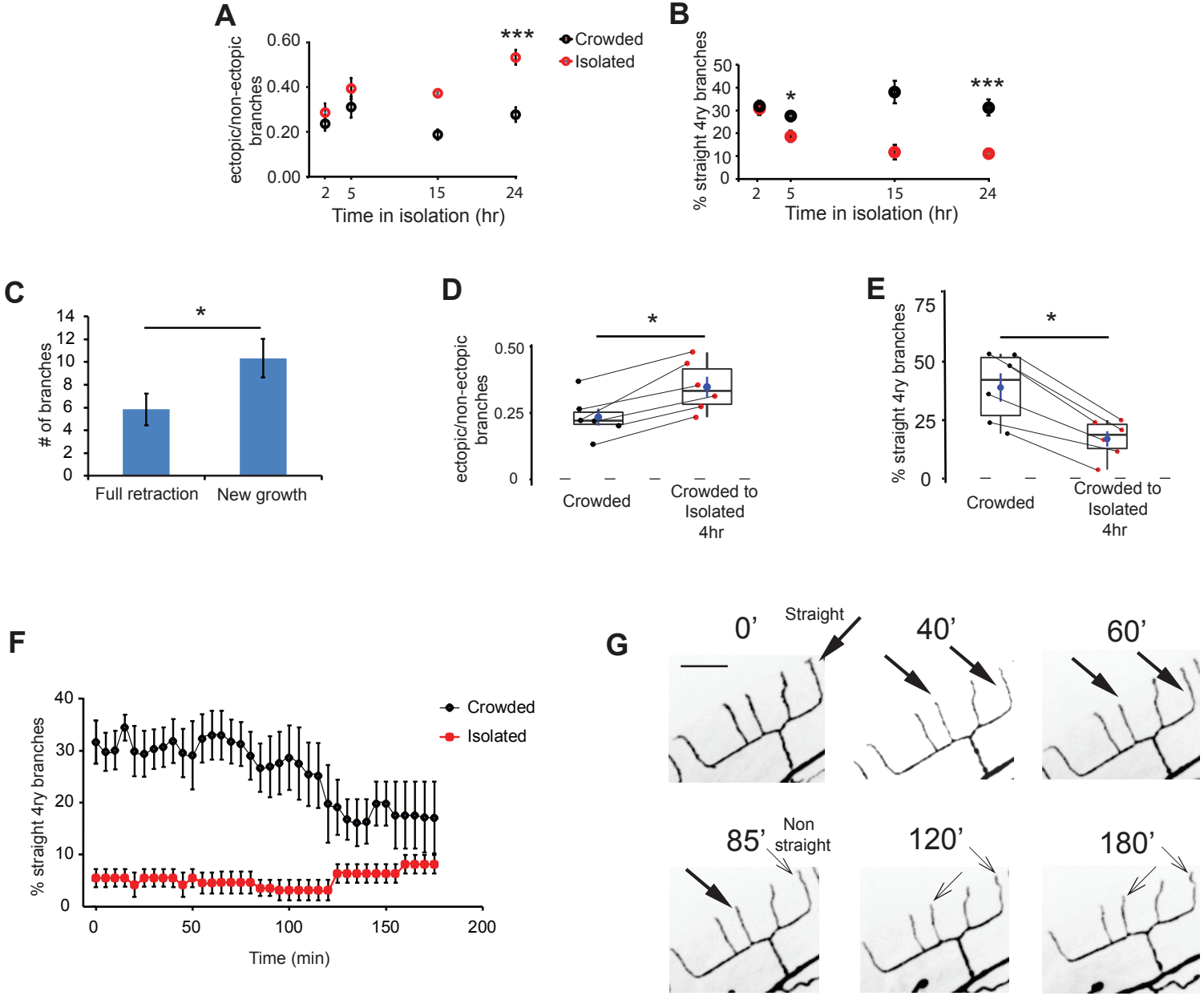
A
ectopic/non-ectopic branches
0.60
0.40
0.20
0.00
2
5
15
24
Time in isolation (hr)
***
Crowded
Isolated
B
% straight 4ry branches
50
40
30
20
10
0
2
5
15
24
Time in isolation (hr)
*
***
C
# of branches
14
12
10
8
6
4
2
0
*
Full retraction
New growth
D
ectopic/non-ectopic branches
0.50
0.25
0
*
Crowded
Crowded to Isolated 4hr
E
% straight 4ry branches
75
50
25
0
*
Crowded
Crowded to Isolated 4hr
F
% straight 4ry branches
40
30
20
10
0
0
50
100
150
200
Time (min)
Crowded
Isolated
G
0'
Straight
40'
60'
85'
Non straight
120'
180'

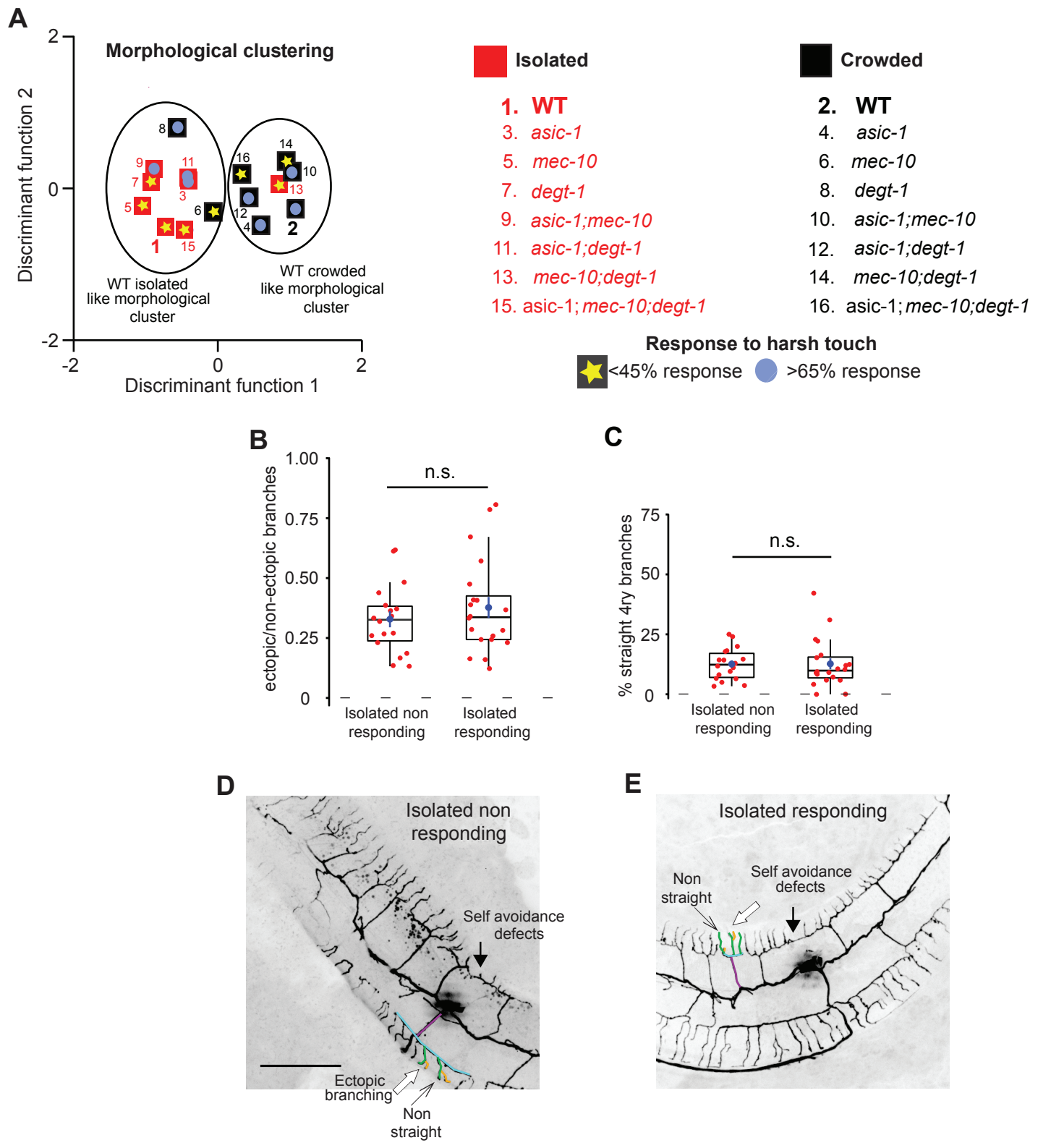
A
Morphological clustering
Discriminant function 2
Discriminant function 1
2
0
-2
-2
0
2
8
9
11
7
3
5
6
1
15
14
16
10
13
12
4
2
WT isolated like morphological cluster
WT crowded like morphological cluster
Isolated
Crowded
1. WT
3. asic-1
5. mec-10
7. degt-1
9. asic-1;mec-10
11. asic-1;degt-1
13. mec-10;degt-1
15. asic-1; mec-10;degt-1
2. WT
4. asic-1
6. mec-10
8. degt-1
10. asic-1;mec-10
12. asic-1;degt-1
14. mec-10;degt-1
16. asic-1; mec-10;degt-1
Response to harsh touch
<45% response
>65% response
B
ectopic/non-ectopic branches
1.00
0.75
0.50
0.25
0
n.s.
Isolated non responding
Isolated responding
C
% straight 4ry branches
75
50
25
0
n.s.
Isolated non responding
Isolated responding
D
Isolated non responding
Self avoidance defects
Ectopic branching
Non straight
E
Isolated responding
Non straight
Self avoidance defects

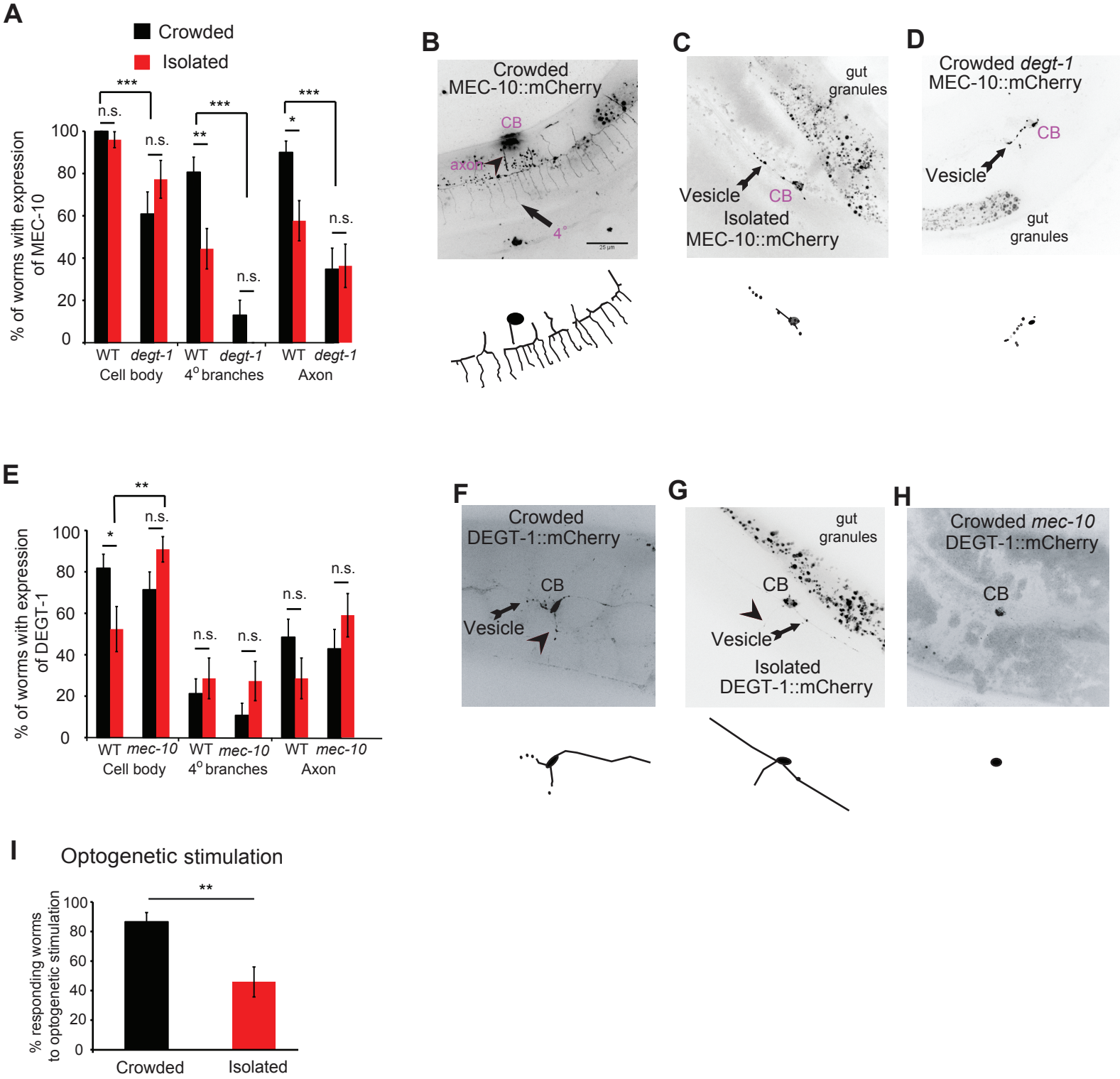
A
Crowded
Isolated
% of worms with expression of MEC-10
100
80
60
40
20
0
***
n.s.
n.s.
***
**
n.s.
***
*
n.s.
WT
degt-1
WT
degt-1
WT
degt-1
Cell body
4° branches
Axon
B
Crowded
MEC-10::mCherry
CB
axon
4°
C
gut granules
Vesicle
CB
Isolated
MEC-10::mCherry
D
Crowded degt-1
MEC-10::mCherry
CB
Vesicle
gut granules
E
% of worms with expression of DEGT-1
100
80
60
40
20
0
**
*
n.s.
n.s.
n.s.
n.s.
n.s.
WT
mec-10
WT
mec-10
WT
mec-10
Cell body
4° branches
Axon
F
Crowded
DEGT-1::mCherry
CB
Vesicle
G
gut granules
CB
Vesicle
Isolated
DEGT-1::mCherry
H
Crowded mec-10
DEGT-1::mCherry
CB
I
Optogenetic stimulation
% responding worms to optogenetic stimulation
100
80
60
40
20
0
**
Crowded
Isolated

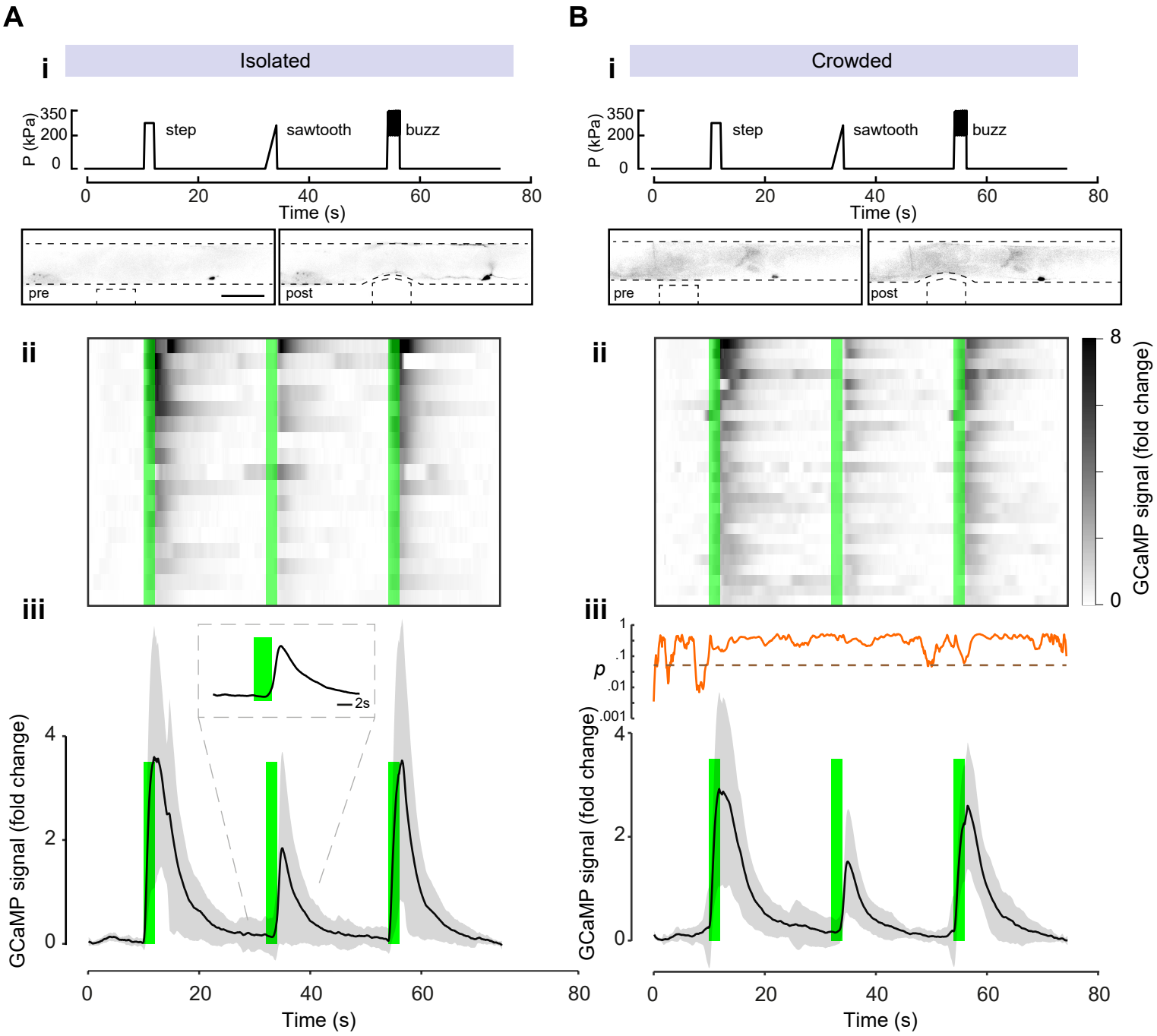
A
i
Isolated
P (kPa)
350
200
0
step
sawtooth
buzz
0
20
40
60
80
Time (s)
pre
post
ii
iii
GCaMP signal (fold change)
4
2
0
2s
Time (s)
B
i
Crowded
P (kPa)
350
200
0
step
sawtooth
buzz
Time (s)
pre
post
ii
8
0
GCaMP signal (fold change)
iii
p
1
.1
.01
.001
GCaMP signal (fold change)
Time (s)

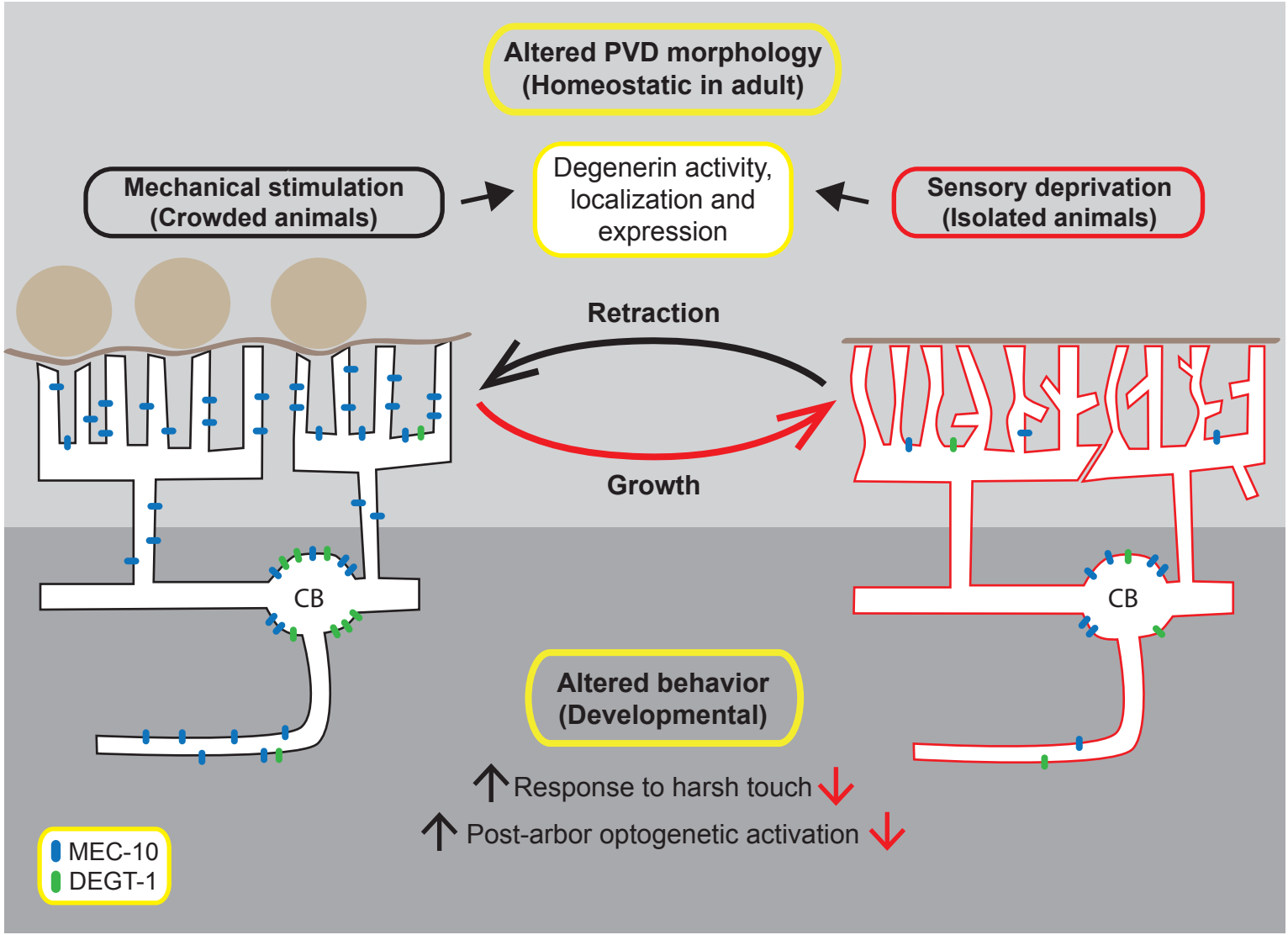
Altered PVD morphology
(Homeostatic in adult)
Mechanical stimulation
(Crowded animals)
Degenerin activity,
localization and
expression
Sensory deprivation
(Isolated animals)
Retraction
Growth
CB
CB
Altered behavior
(Developmental)
Response to harsh touch
Post-arbor optogenetic activation
MEC-10
DEGT-1

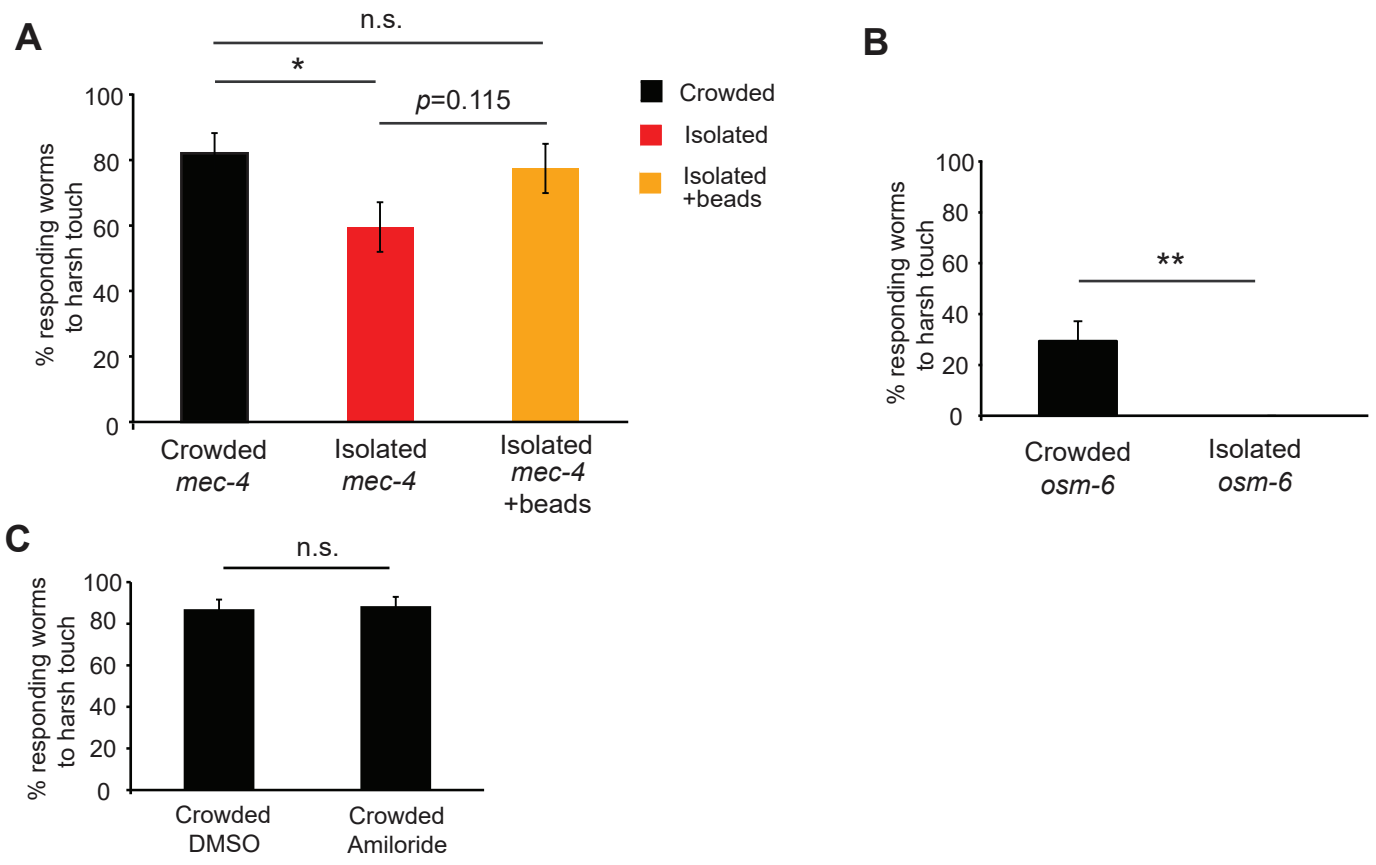
A
n.s.
*
p=0.115
100
80
60
40
20
0
% responding worms to harsh touch
Crowded
Isolated
Isolated +beads
Crowded mec-4
Isolated mec-4
Isolated mec-4 +beads
B
100
80
60
40
20
0
% responding worms to harsh touch
**
Crowded osm-6
Isolated osm-6
C
n.s.
100
80
60
40
20
0
% responding worms to harsh touch
Crowded DMSO
Crowded Amiloride

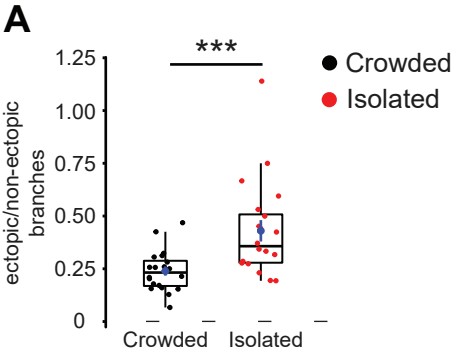
A
***
Crowded
Isolated
ectopic/non-ectopic branches
1.25
1.00
0.75
0.50
0.25
0
Crowded
Isolated

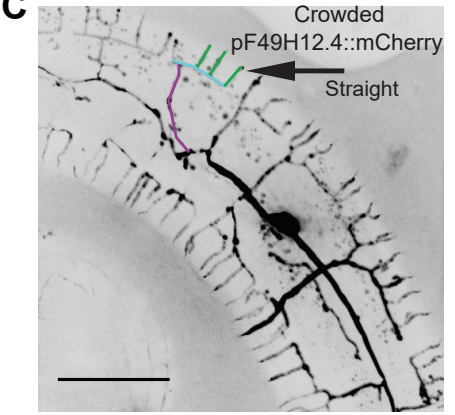
C
Crowded
pF49H12.4::mCherry
Straight

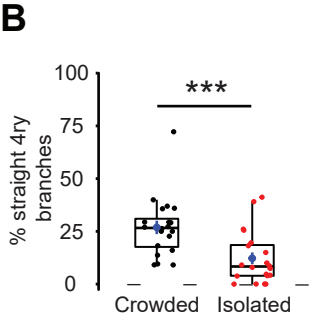
B
***
% straight 4ry branches
100
75
50
25
0
Crowded
Isolated

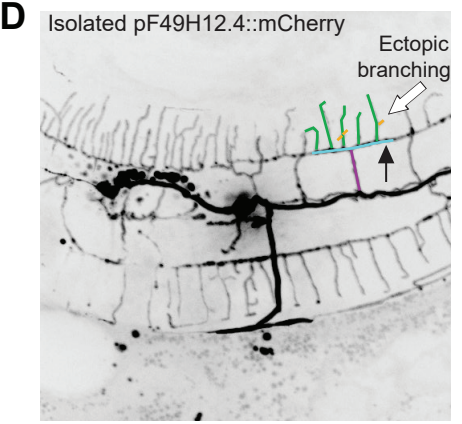
D
Isolated pF49H12.4::mCherry
Ectopic branching

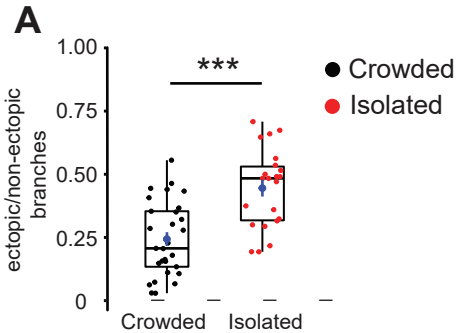
A
1.00
0.75
0.50
0.25
0
ectopic/non-ectopic branches
***
Crowded
Isolated
Crowded
Isolated

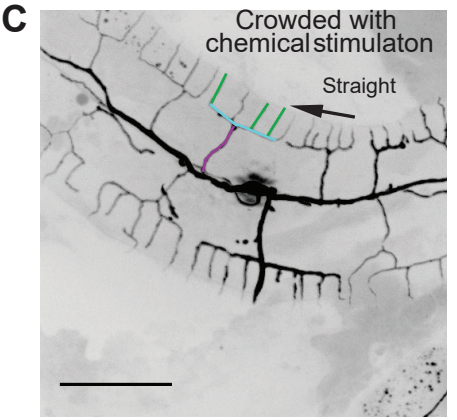
C
Crowded with chemical stimulaton
Straight

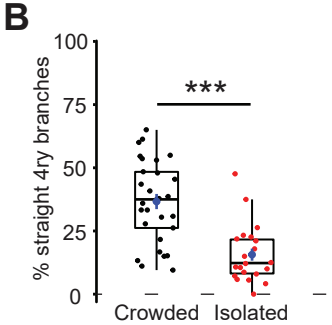
B
100
75
50
25
0
% straight 4ry branches
***
Crowded
Isolated

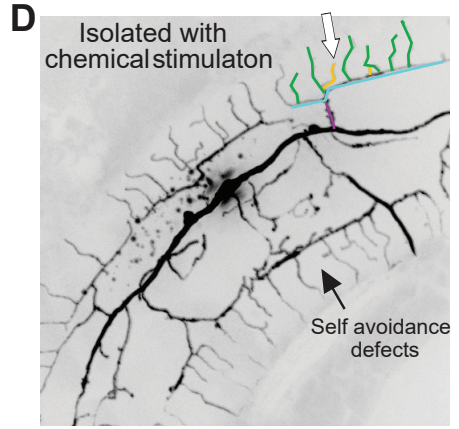
D
Isolated with chemical stimulaton
Self avoidance defects

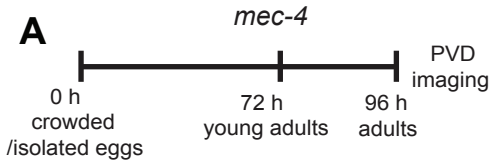
A
mec-4
PVD imaging
0 h
crowded
/isolated eggs
72 h
young adults
96 h
adults

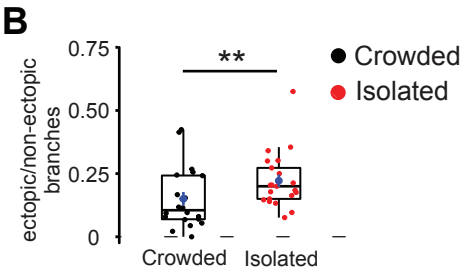
B
ectopic/non-ectopic branches
0.75
0.50
0.25
0
**
Crowded
Isolated
Crowded
Isolated

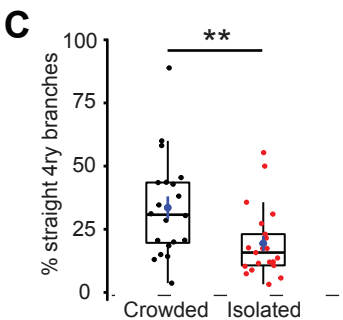
C
% straight 4ry branches
100
75
50
25
0
**
Crowded
Isolated

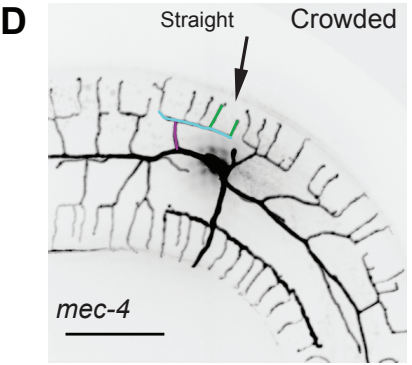
D
Straight
Crowded
mec-4

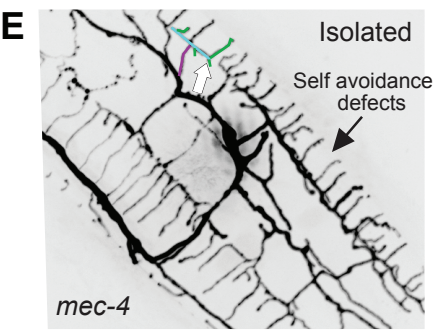
E
Isolated
Self avoidance defects
mec-4

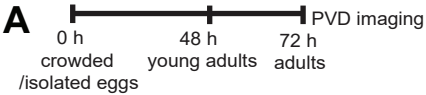
A
PVD imaging
0 h
crowded
/isolated eggs
48 h
young adults
72 h
adults

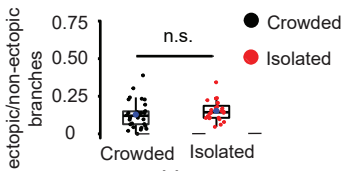
B
ectopic/non-ectopic branches
0.75
0.50
0.25
0
n.s.
Crowded
Isolated
Crowded
Isolated

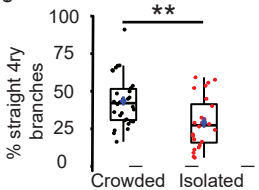
C
% straight 4ry branches
100
75
50
25
0
**
Crowded
Isolated

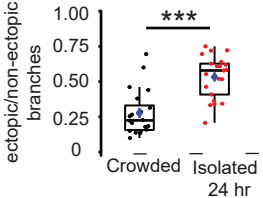
F
ectopic/non-ectopic branches
1.00
0.75
0.50
0.25
0
***
Crowded
Isolated
24 hr

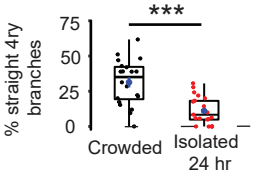
G
% straight 4ry branches
75
50
25
0
***
Crowded
Isolated
24 hr

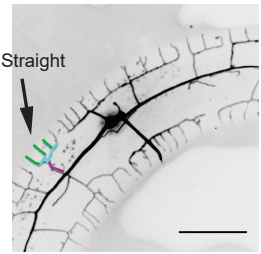
D
Straight

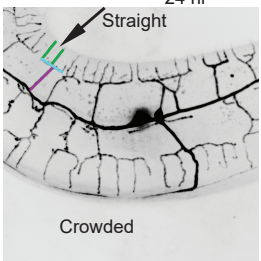
H
Straight
Crowded

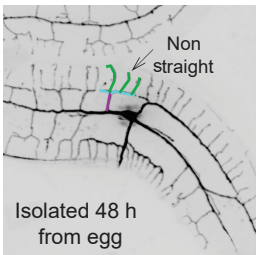
E
Non
straight
Isolated 48 h
from egg

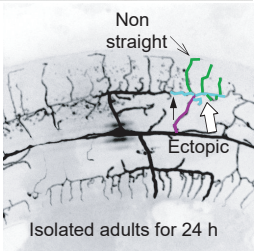
I
Non
straight
Ectopic
Isolated adults for 24 h

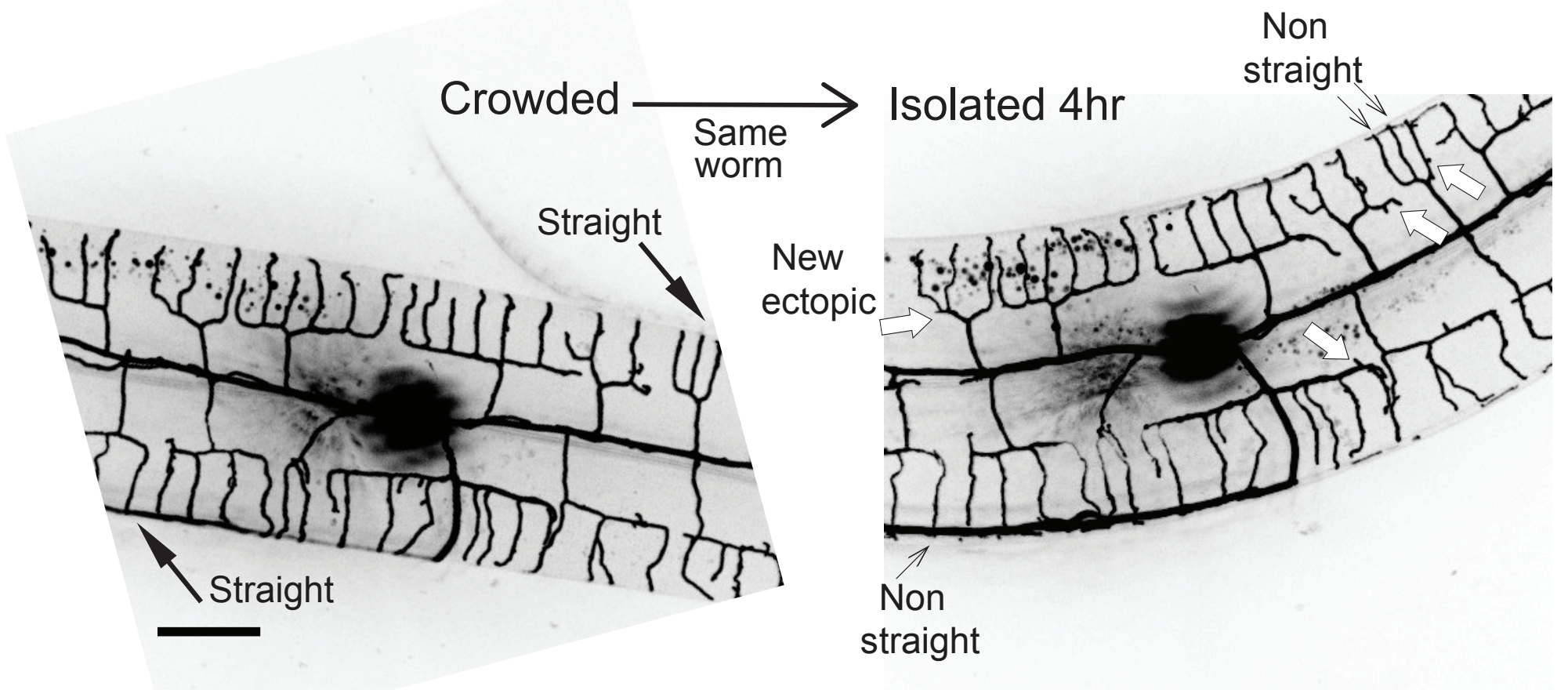
Crowded
Same worm
Isolated 4hr
Straight
Straight
New ectopic
Non straight
Non straight

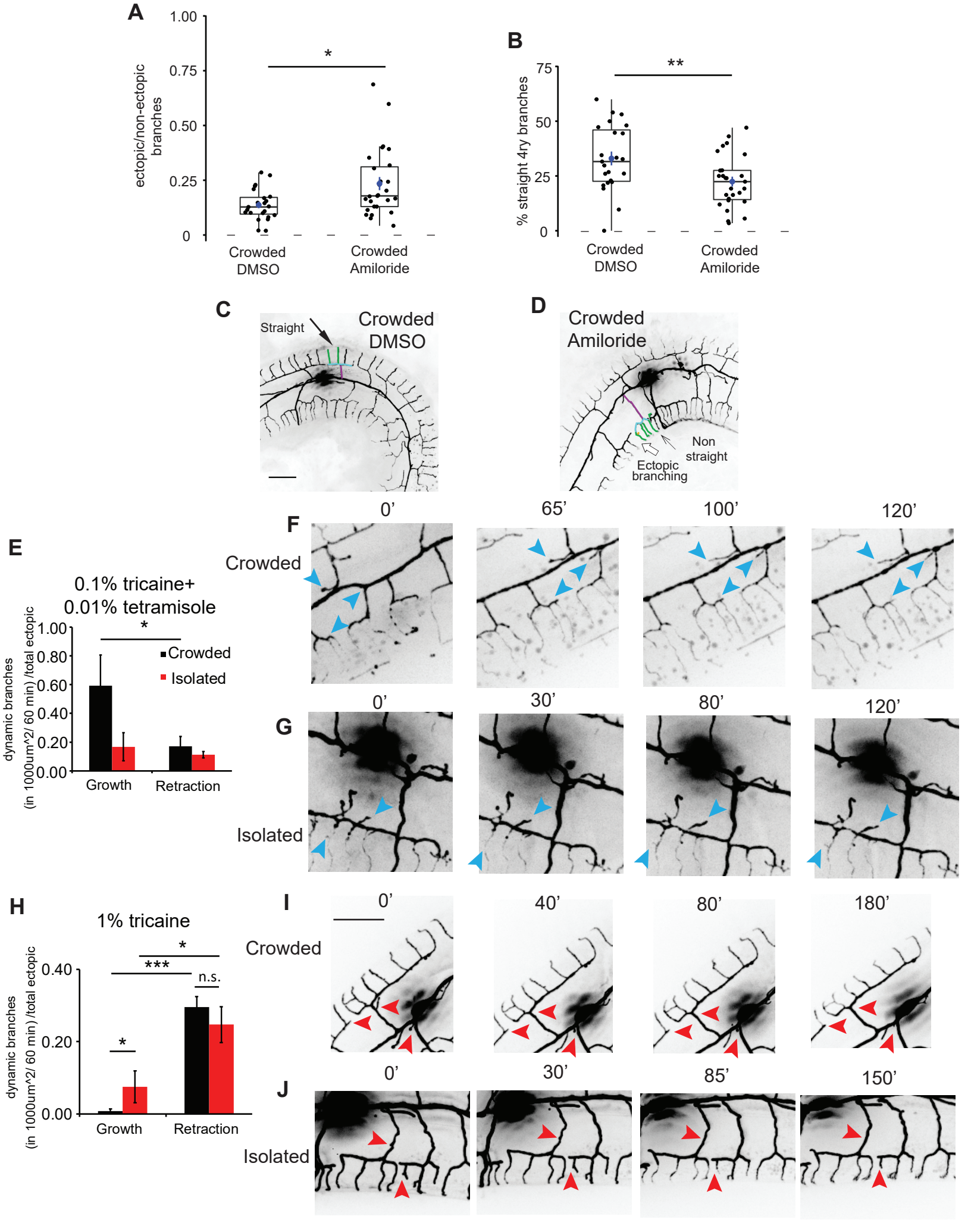
A
ectopic/non-ectopic branches
1.00
0.75
0.50
0.25
0
*
Crowded DMSO
Crowded Amiloride
B
% straight 4ry branches
75
50
25
0
**
Crowded DMSO
Crowded Amiloride
C
Straight
Crowded DMSO
D
Crowded Amiloride
Non straight
Ectopic branching
E
0.1% tricaine+
0.01% tetramisole
dynamic branches (in 1000um^2/ 60 min) /total ectopic
1.00
0.80
0.60
0.40
0.20
0.00
*
Crowded
Isolated
Growth
Retraction
F
Crowded
0'
65'
100'
120'
G
Isolated
0'
30'
80'
120'
H
1% tricaine
dynamic branches (in 1000um^2/ 60 min) /total ectopic
0.40
0.20
0.00
*
***
n.s.
*
Growth
Retraction
I
Crowded
0'
40'
80'
180'
J
Isolated
0'
30'
85'
150'

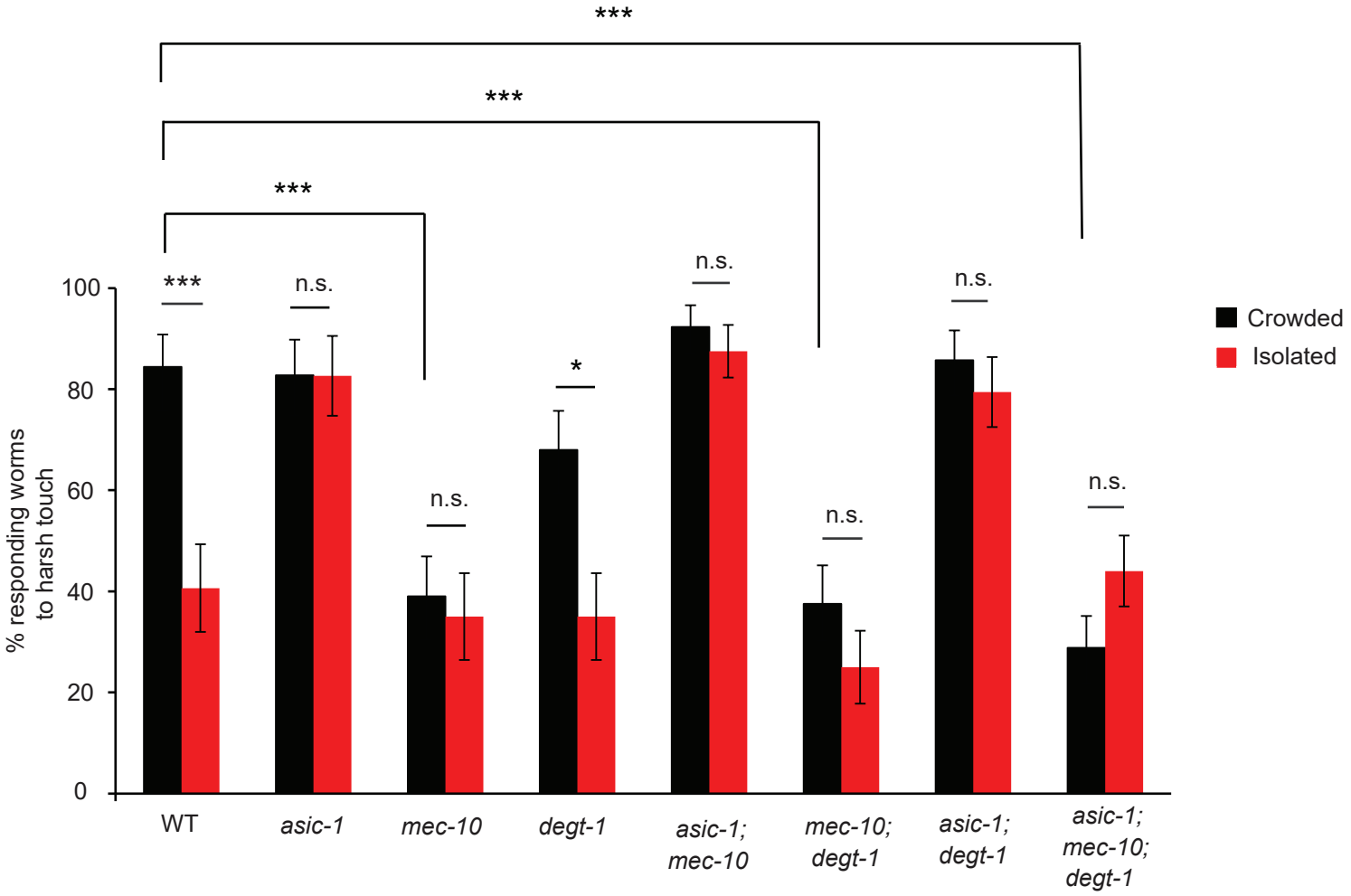
***
***
***
***
n.s.
n.s.
*
n.s.
n.s.
n.s.
n.s.
100
80
60
40
20
0
% responding worms to harsh touch
Crowded
Isolated
WT
asic-1
mec-10
degt-1
asic-1; mec-10
mec-10; degt-1
asic-1; degt-1
asic-1; mec-10; degt-1

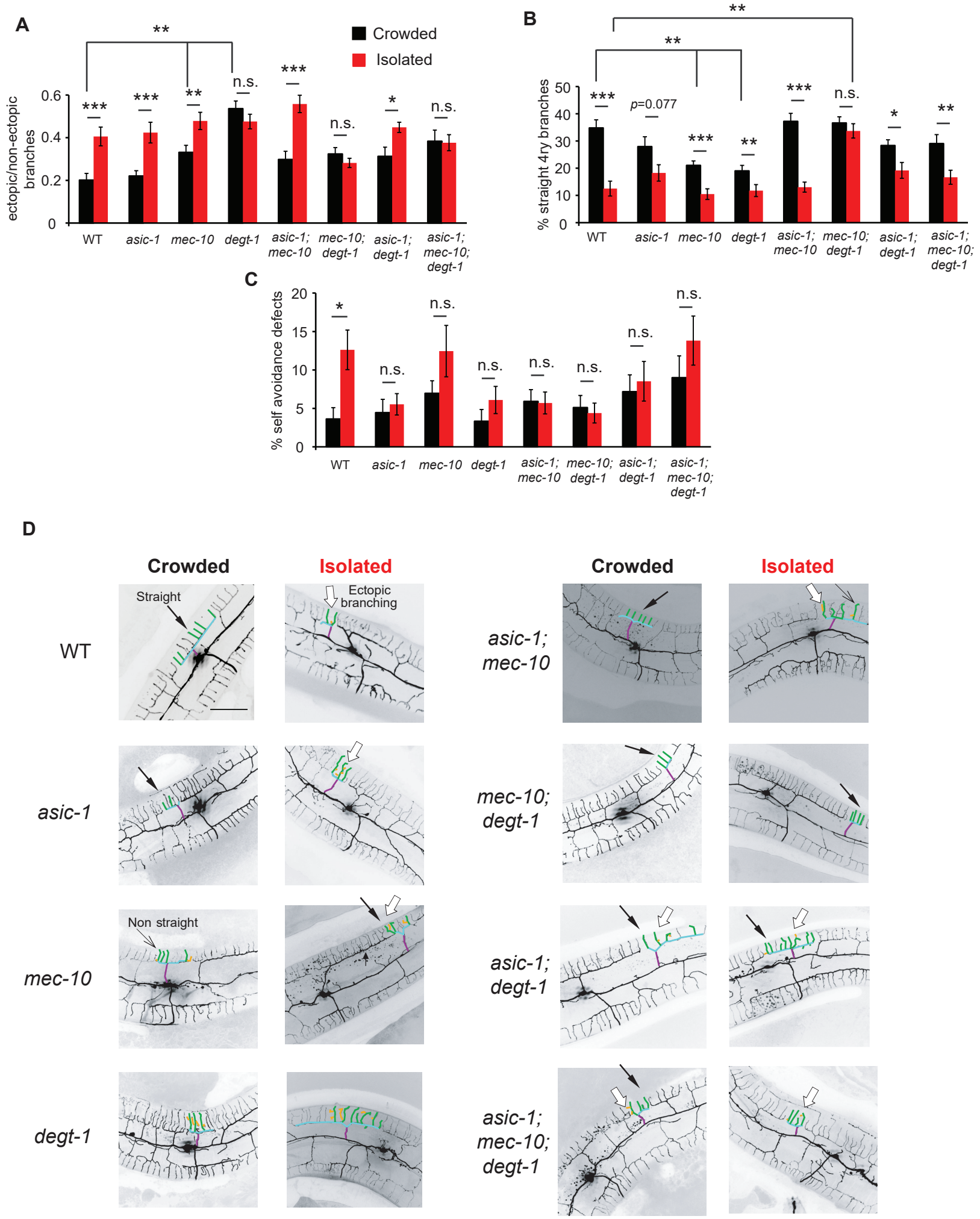
A
Crowded
Isolated
ectopic/non-ectopic branches
0.6
0.4
0.2
0
**
***
***
**
n.s.
***
n.s.
*
n.s.
WT
asic-1
mec-10
degt-1
asic-1; mec-10
mec-10; degt-1
asic-1; degt-1
asic-1; mec-10; degt-1
B
% straight 4ry branches
50
40
30
20
10
0
**
**
***
p=0.077
***
**
***
n.s.
*
**
C
% self avoidance defects
20
15
10
5
0
*
n.s.
n.s.
n.s.
n.s.
n.s.
n.s.
D
Crowded
Isolated
Straight
Ectopic branching
WT
asic-1
Non straight
mec-10
degt-1
asic-1; mec-10
mec-10; degt-1
asic-1; degt-1
asic-1; mec-10; degt-1

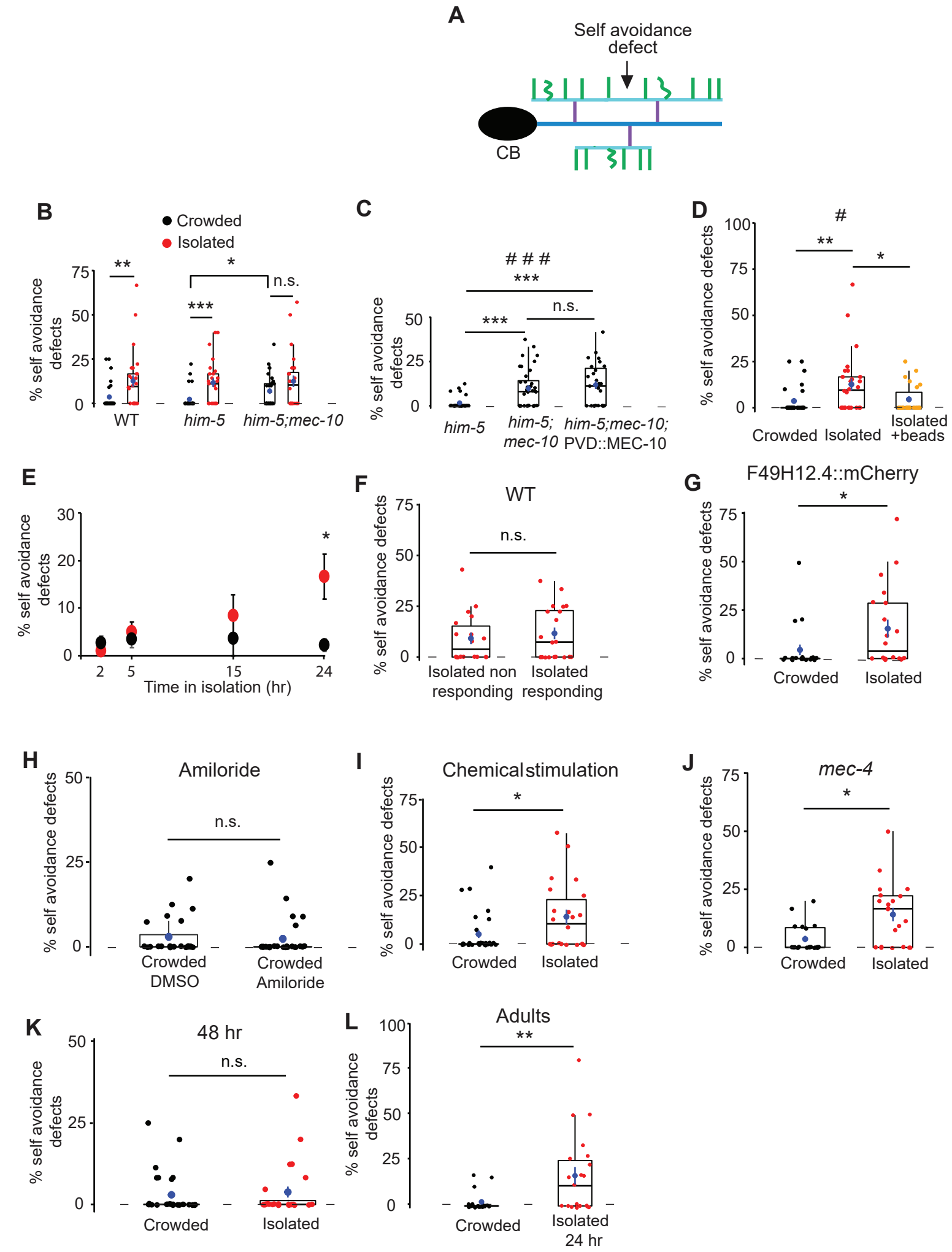
A
Self avoidance defect
CB
B
Crowded
Isolated
% self avoidance defects
WT
him-5
him-5;mec-10
n.s.
C
# # #
him-5
him-5; mec-10
him-5;mec-10; PVD::MEC-10
D
#
Crowded
Isolated
Isolated +beads
E
Time in isolation (hr)
F
WT
Isolated non responding
Isolated responding
G
F49H12.4::mCherry
H
Amiloride
Crowded DMSO
Crowded Amiloride
I
Chemical stimulation
J
mec-4
K
48 hr
L
Adults
Isolated 24 hr

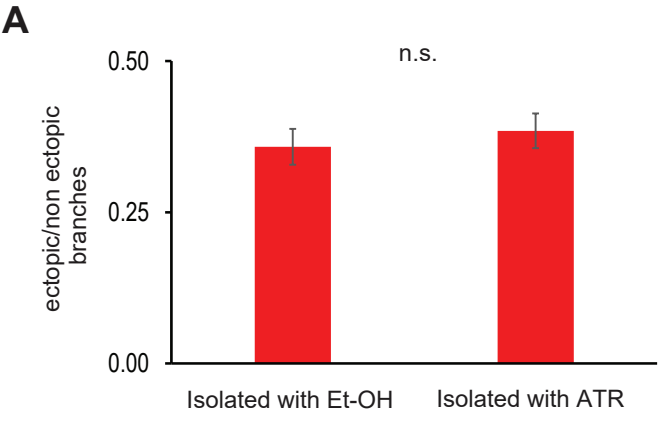
A
n.s.
0.50
0.25
0.00
ectopic/non ectopic branches
Isolated with Et-OH
Isolated with ATR

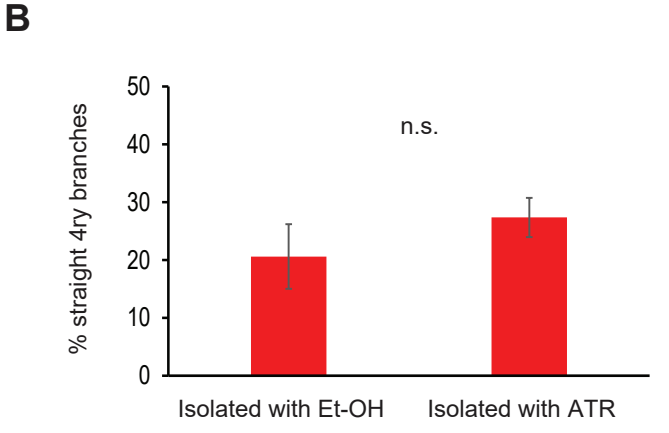
B
n.s.
50
40
30
20
10
0
% straight 4ry branches
Isolated with Et-OH
Isolated with ATR

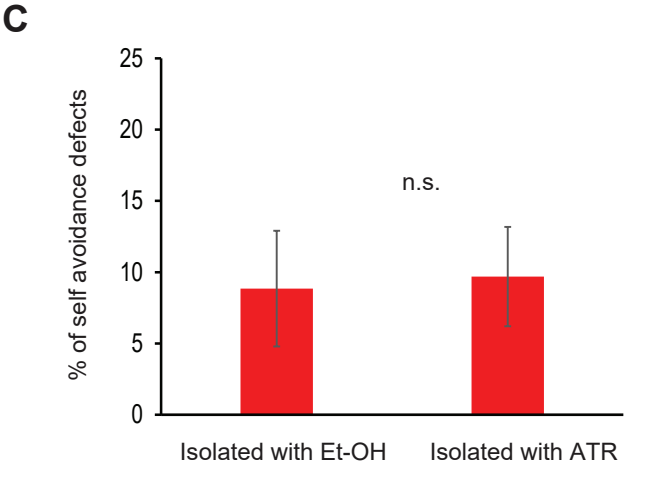
C
n.s.
25
20
15
10
5
0
% of self avoidance defects
Isolated with Et-OH
Isolated with ATR

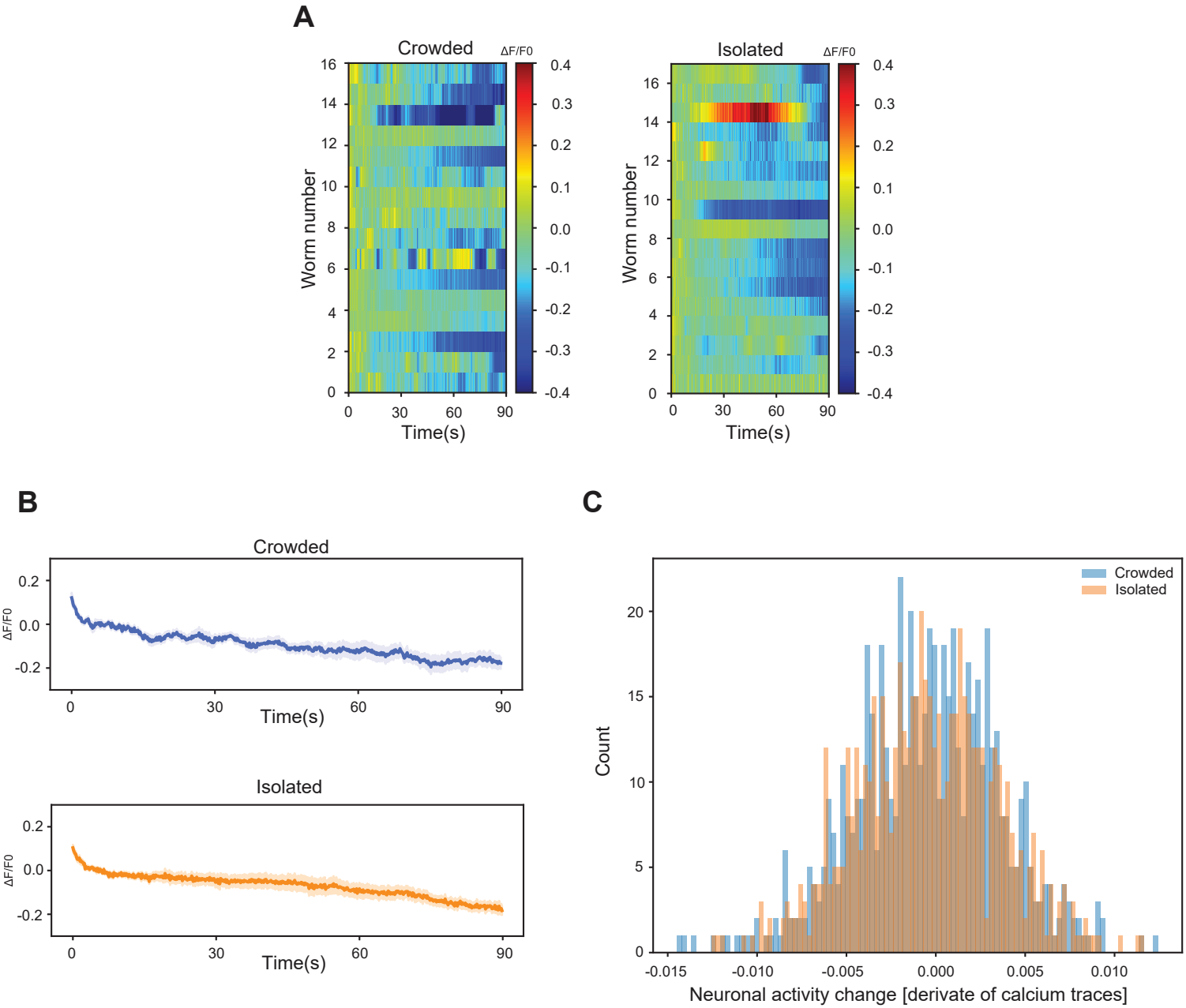
A
Crowded
Isolated
ΔF/F0
Worm number
Time(s)
B
Crowded
Isolated
ΔF/F0
Time(s)
C
Crowded
Isolated
Count
Neuronal activity change [derivate of calcium traces]

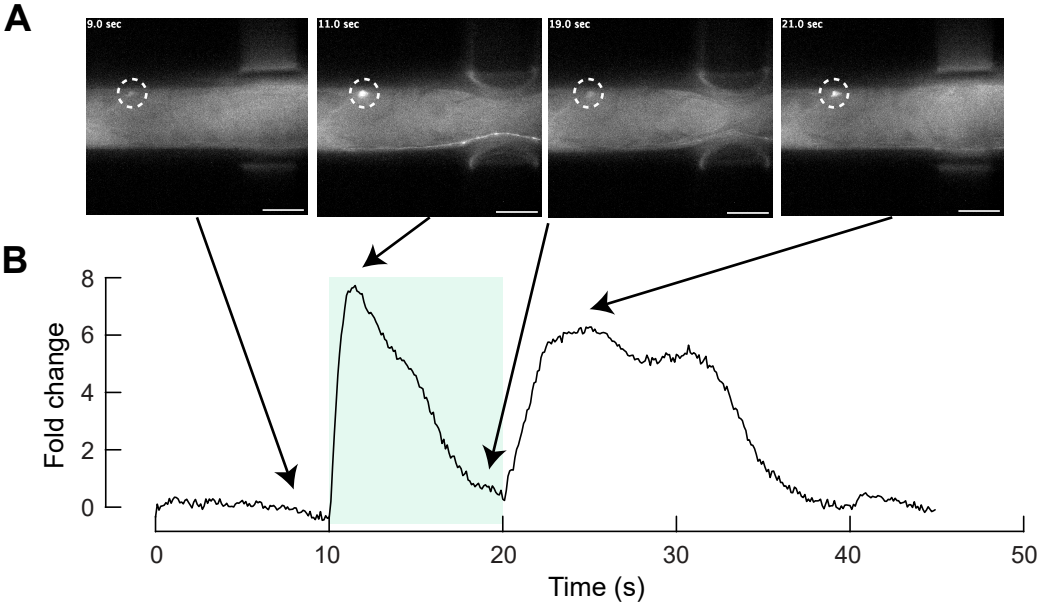
A
9.0 sec
11.0 sec
19.0 sec
21.0 sec
B
Fold change
8
6
4
2
0
0
10
20
30
40
50
Time (s)

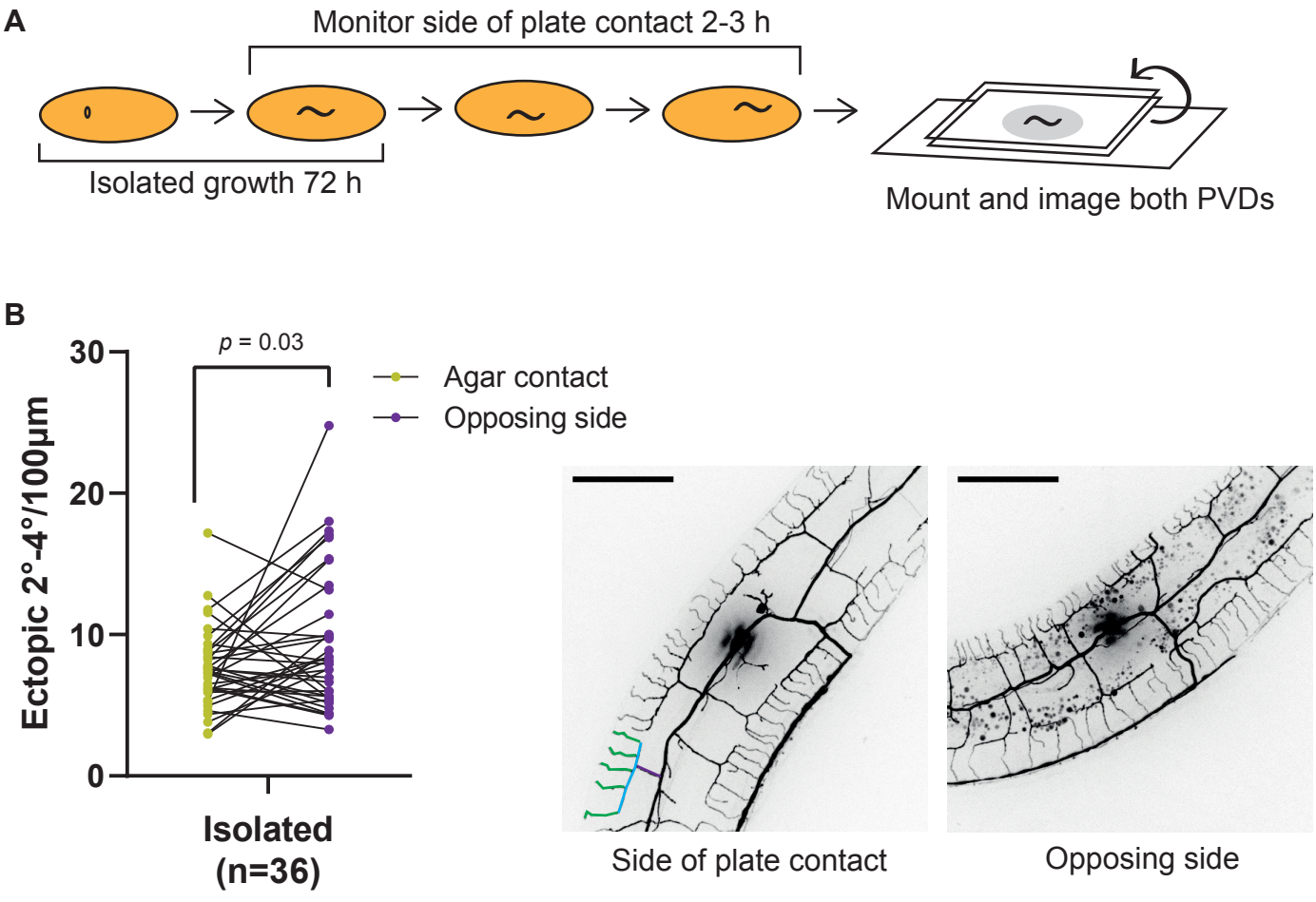
A
Monitor side of plate contact 2-3 h
Isolated growth 72 h
Mount and image both PVDs
B
p = 0.03
Agar contact
Opposing side
Ectopic 2°-4°/100µm
30
20
10
0
Isolated
(n=36)
Side of plate contact
Opposing side